Targeting *Leishmania donovani* Sphingosine Kinase 1 using PF-543 enhances immune response and limits parasite load

Short Title: Targeting Sphingosine-1-phosphate kinase to limit *Leishmania* growth

Evanka Madan[1,2], Ruby Bansal[1], Jhalak Singhal[1], Monica Saini[3], Sadat Shafi[1,4], Nishant Joshi[5], Shailja Singh[1*]

[1]Special Centre for Molecular Medicine, Jawaharlal Nehru University, New Delhi 110067, India

[2]Department of Biotechnology and Research, Sir Ganga Ram Hospital, New Delhi-110008, India

[3]Biology Centre Czech Academy of Sciences, Institute of Parasitology, Laboratory of RNA Biology of Protists, Czech Republic

[4]Department of Pharmacology, School of Pharmaceutical Education and Research, Jamia Hamdard, New Delhi, India.

[5] Eli Lilly Services India Private Limited, Bengaluru, Karnataka 560103

email addresses of authors:

Evanka Madan: evanka.madan@gmail.com

Ruby Bansal: rubybansal1242@gmail.com

Jhalak Singhal: jhalakbiotech@gmail.com

Monica Saini: monikabcas@gmail.com

Sadat Shafi: sadatshafi2016@gmail.com

Nishant Joshi: nj633@snu.edu.in

Correspondence:

∗Shailja Singh; Special Centre for Molecular Medicine, Jawaharlal Nehru University, Delhi, 110067, India; shailja.jnu@gmail.com

Abstract

Background

Sphingosine-1-phosphate (S1P) is a bioactive lipid mediator regulating apoptosis, proliferation, and immune responses. While S1Ps presence in *Leishmania donovani* phagolysosomes has been reported, the role of sphingosine kinases, especially SphK1, in parasite survival and host immune modulation remains underexplored. This study investigates the molecular and functional role of *L. donovani* SphK1 (*Ld*SphK1) and evaluates the antileishmanial potential of PF-543, a specific SphK1 inhibitor.

Methods

*Ld*SphK1 and human SphK1 (*rh*SphK1) were cloned, expressed in *E. coli*, purified, and analyzed by SDS-PAGE. Enzymatic activity and inhibition by PF543 were assessed using NBD-S1P-based fluorometric assays. Protein-ligand interactions were analyzed using Microscale Thermophoresis (MST). *Leishmania* promastigotes overexpressing *Ld*SphK1 were studied via confocal microscopy, and their viability and infectivity were assessed *in vitro*. THP-1 macrophages infected with *L. donovani* were treated with PF543 alone or with Amphotericin B and analyzed by MTT assay, RT-PCR, Giemsa staining, ELISA and immunoblotting. *In vivo* efficacy was tested in *L. donovani*-infected Swiss mice.

Results

*rLd*SphK1 (~102 kDa) and *rh*SphK1 (~50 kDa) were enzymatically active and significantly inhibited by PF-543. MST confirmed high-affinity binding of PF-543 (KD ~29 microMolar). In *L. donovani* SphK1 overexpressor *(Ld*SphKa) promastigotes, PF543 inhibited SphK1 activity and reduced parasite infectivity, more than in wildtype *L. donovani* promastigotes. Notably, PF543 treatment reduced parasite infectivity *in vitro*, lowered amastigote load by ~40%, and promoted a pro-inflammatory cytokine shift (↑IL-12, ↑TNF-α, ↓IL-10). Inhibition

of ceramide synthesis and S1P supplementation revealed that S1P rescues ceramide-induced parasite death, implicating SphK1 in parasite survival. PF543 and Amphotericin B demonstrated synergistic anti-parasitic effects both *in vitro* and *in vivo*, with >90% reduction in parasite burden in mice.

Conclusion

PF543 is a potent inhibitor of SphK1, impairing parasite survival and modulating host immune responses. When combined with Amphotericin B, it offers a synergistic therapeutic strategy against visceral leishmaniasis, warranting further clinical exploration.

Keywords: SphK-1, PF-543, Amphotericin B, *Leishmania donovani,* THP-1

Author Summary

Leishmaniasis, a neglected tropical disease, has limited available treatments and is becoming more resistant to medications. In this study, we explored the therapeutic potential of PF-543, a potent sphingosine kinase 1 (SphK1) inhibitor (demonstrated anticancer effects in various preclinical models) against *Leishmania donovani*. We successfully cloned and purified both *Leishmania* and human SphK1 proteins and confirmed PF-543 binding through biochemical and biophysical assays. Overexpression of *Ld*SphK1 in parasites enhanced their survival and infectivity. *In vitro,* PF-543 treatment of infected macrophages decreased amastigote burden, shifted cytokine profiles towards a pro-inflammatory state, and enhanced host cell apoptosis. Notably, PF-543 acted synergistically with Amphotericin B, the current clinical drug, both *in vitro* and *in vivo* in Swiss mice, drastically lowering parasite burden. This study highlights the possibility of combination therapy and finds PF-543 to be a promising irresistible host-targeted antileishmanial drug.

82 **Introduction**

83 Leishmaniasis is a neglected tropical disease caused by intracellular protozoa parasite
84 *Leishmania* [1]. It invades macrophages and selectively impairs host's critical signaling
85 pathways for its successful intracellular growth and proliferation [2]. In particular, alteration
86 in lipid metabolic pathways, lipid relocation, accumulation and mitochondrial dysfunction
87 during *Leishmania* infection has been proven to be a critical step in the progression of disease
88 [3].

89 Decrease in efficiency of current anti-leishmanial agents, increase in cost and complexity of
90 curing *Leishmania*, increased parasitic resistance to the chemicals and limited number of
91 available anti-leishmanial drugs has spur the research for novel approaches [4] Pentavalent
92 antimonials (sodium stibogluconate and meglumine antimoniate), liposomal amphotericin B,
93 Miltefosine and Paromomycin are the current drugs for Visceral Leishmaniasis [5,6]. However,
94 resistance has been seen in endemic regions, where these drugs are extensively used, with risk
95 of serious cardiotoxicity, toxic effects on the kidneys, leading to death [6,7]. The need for
96 novel, effective, and safer therapeutic alternatives is therefore urgent.

97 In this context, targeting host or parasite-encoded enzymes has emerged as the promising
98 strategy for identifying new anti-leishmanial agents. For the first time, we explored the
99 potential of PF-543, a potent Sphingosine kinase (SphK) inhibitor to modulate Sphingosine-1-
100 phosphate (S1P) signalling, and disrupt *Leishmania* infection. Interestingly, evidences have
101 suggested a key role for SphK in several lung pathologies, including lung fibrosis, pulmonary
102 artery hypertension, asthma, ischemia reperfusion injury [8-12]. Recent studies have also
103 implicated S1P signaling in the biology of *Leishmania donovani,* especially within
104 phagolysosomes [13].

105 Among the two SphK isoforms, SphK1 is more responsive to various stimuli and is
106 increasingly viewed as a favourable therapeutic target compared to the more constitutively

107 active SphK2 [14]. Our work focused on modulating SphK1, a key enzyme in conversion of
108 sphingosine to SIP, which is critical for parasite survival and host immune evasion. Notably,
109 SphK1 enables *Leishmania* to manage toxic metabolites, endure cellular stress, and establish
110 infection, making it a compelling drug target [15].

111 These days, there are growing interests in using small-molecule inhibitors of the Sphingosine
112 kinases (SphK1 and SphK2) as potential therapeutics or preventive agents for human diseases
113 [16]. The SphK inhibitors: N, N-dimethyl-sphingosine (DMS), SKI-5C and PF-543 are
114 formerly developed as antitumoral drugs [17]. We hypothesize that targeting both host and
115 parasite SphK1 with these inhibitors, especially PF-543, could suppress parasite survival
116 within macrophages and may serve as a novel therapeutic approach to the classical treatments
117 against *Leishmania.*

118 Till date, there is no study addressing the role of PF-543 in sensing SIP signalling and inducing
119 lysosomal stress in human macrophages infected with *Leishmania*, so, we sought to study the
120 underlying molecular pathways of these SphK inhibitors involved in parasite survival,
121 including the role of ceramide accumulation and intracellular calcium dysregulation, which are
122 known to contribute to parasite death via ER stress and autophagy [18-21].

123 Notably, both *Leishmania* and macrophages are known to harbor SphK1, making PF-543 a
124 unique dual-target inhibitor. Importantly, PF-543-mediated inhibition of host SphK1 appears
125 safe due to the compensatory presence of SphK2, further minimizing potential side effects and
126 reducing the likelihood of resistance—since the drug targets a host rather than a parasite
127 protein.

128 In this study, we cloned and expressed *Leishmania* and human SphK1, confirmed protein
129 purification, and validated PF-543 binding through Microscale Thermophoresis (MST), *in*
130 *silico* docking, and kinetic analysis. In *Leishmania* promastigotes, SphK1 was overexpressed
131 and checked for SphK1 activity, parasite infectivity, inflammatory responses following PF-543

treatment. Mechanistic studies explored the role of ceramide and autophagy, while potential impact of Amphotericin B, the current drug used in clinics alone and in combination with PF-543 against *L. donovani* promastigotes, amastigotes and Swiss mice was evaluated.

Usage of Amphotericin B liposome as anti-leishmanial is already published [22] and patented [23]. PF-543, the most potent SphK1 inhibitor developed by Pfizer, is not yet known to be an anti-leishmanial drug. Here, for the first time, we report the anti-leishmanial potential of PF-543, both as standalone agent and in combination with Amphotericin B as a new anti-leishmanial formulation.

By leveraging host-targeted mechanisms and minimizing the risk of drug resistance, the PF-543 and Amphotericin B combination introduces a promising new direction in leishmaniasis treatment. These findings not only provide insight into host-parasite interactions but also open up new avenues for exploiting host pathways to combat parasitic diseases.

Methods

In silico search for SphK1 like protein in Leishmania donovani

An *in-silico* search was conducted in the Kinetoplastid database TriTrypDB (www.tritrypdb.org) to identify any homologous protein similar to prokaryotic SphK1 in *Leishmania donovani* [24]. Sequence alignments and identity computations were conducted using ClustalW [25]. Homologues of SphK1 from *L. donovani*, along with other prokaryotes and eukaryotes were analyzed using the Molecular Evolutionary Genetics Analysis (MEGAX) tool [26]. The evolutionary trajectory was determined using the Neighbor-Joining method. The bootstrap consensus tree was generated from replicates and the evolutionary distances were calculated using the Poisson correction method. Pymol was utilized to align the two structures and compute the RMSD post-alignment [27].

156 ***In-silico docking studies***

157 The protein structure of hSphK1 (Uniprot ID- Q9NYA1), a protein derived from H. sapiens,
158 was retrieved from the protein data bank [28,29]. Protein structure of *L. donovani* sequence
159 *Ld*SphK (*Ld*SphK_260680.1.1) was obtained from TriTrypDB [30]. Phyre2 web server was
160 used for homology 3D protein modelling of the protein and Procheck sever was used for
161 Ramachandran plot analysis of the model [31,32]. The Swiss PDB viewer and ChemBio Draw
162 ultra 3D software were used to optimize the structure of proteins and ligands [33,34]. The
163 process of molecular docking between molecule PF-543 and hSphK1 was conducted using
164 Autodock version 4.2 and Cygwin terminal version 3.1 software [35,36]. The residues located
165 in the vicinity of the binding pocket were selected to create a grid (with a spacing of 0.375)
166 centred at coordinates X-51.488, Y-53.406, Z- -1.49 for hSphK1 and X-4.021, Y- -21.535, Z-
167 15.254 for *Ld*SphK1 respectively. This grid was used to facilitate the binding of the ligand.
168 The docking data were further analyzed and visualized using the PLIP, Ligplot+ version 2.2,
169 Discovery Studio version 19.1.0, and Pymol version 2.3.2 software tools [37–40].

170 ***Cloning and recombinant protein purification of LdSphk1***

171 Nucleotide sequence encoding full length sequence of *L. donovani* Sphk1 (1-2808 bp, **Fig S1A**)
172 was selected for recombinant protein generation as a fusion protein with an N-terminal 6x-
173 Histidine-tag using the vector pET-28 a(+) vector. DNA fragment for the gene cloning was
174 PCR amplified from genomic DNA of *L. donovani* using the following primer pair:
175 *Ld*Sphk1_BamHI_FP 5'-GATGGGATCCATGCACTCTTTCACCTCCAA-3' and
176 *Ld*Sphk1_XhoI_RP 5'-ATTCTCGAGCTACCCACTGCGCACGAGCT-3'with Phusion™
177 High-Fidelity DNA Polymerase (Thermo Scientific, US). The amplified DNA fragment was
178 purified with QIAquick Gel Extraction Kit (Qiagen) using the manufacturer's protocol.

179 Purified *Ld*Sphk1 insert and the expression vector pET-28 a(+) were digested with
180 BamHI/XhoI restriction enzymes (New England Biolabs, UK), and were ligated overnight at
181 16°C using T4 DNA ligase (New England Biolabs, UK). The ligation mix was transformed
182 into *E. coli* DH5-α competent cells (*E.Coli* DH5-α cells were obtained from ThermoFisher
183 Scientific, USA Catalog number C0112) and positive clones were screened by colony PCR
184 followed by confirmation of the cloned plasmid with BamHI/XhoI restriction digestion **(Fig**
185 **S1B)** and further transformed in Rossetta *E. coli* (Rossetta *E. coli* were obtained from Sigma-
186 Aldrich, USA with Catalog number 71397) expression strain for *Ld*Sphk1 recombinant protein
187 expression **(Fig S1C).** For recombinant protein induction, the cells were induced with 1mM
188 IPTG for 4 hours at 37°C in Terrific broth. Purification of recombinant protein was achieved
189 by affinity chromatography.
190 The *rLd*SphK1 protein (amino acid sequence for the protein shown in **Fig S2A**) was eluted
191 after addition of 150mM and 250mM imidazole solution. The eluted fractions were analysed
192 by running on 12% SDS PAGE and the fractions containing pure protein were pooled and
193 concentrated using a centricon device, followed by buffer exchange with PBS. Since most of
194 the protein was localized in the inclusion bodies, we purified the protein from inclusion bodies
195 under denaturation conditions. Briefly, inclusion bodies were obtained after sonication and
196 subsequent centrifugation at 13,000 rpm and solubilized in urea buffer composed of 8M urea,
197 20mM Tris, 250mM NaCl with pH 8.0 and subsequently incubated with Ni-NTA beads
198 (Qiagen, Germany) overnight for binding. The beads were then loaded in gravity flow column
199 (Qiagen, Germany). Further, *Ld*SphK1 protein bound with the beads was then eluted by 10mM,
200 25mM, 50mM, 100mM, 250mM and 500mM imidazole solutions prepared in urea buffer.
201 Eluted fractions containing pure protein were pooled and refolded by dialyzing against
202 refolding buffer composed of 100mM Tris, 20% Glycerol, 250mM L-Arg, 1mM EDTA, 1mM

203 GSG and 0.5mM GSSG with pH 8.0. Refolded protein was reconstituted in PBS (pH 7.4) and
204 concentrated using centricon tubes with 10kDa cut-off (Merck, Germany).

205 ***Recombinant protein purification of HumanSphk1***

206 CDS encoding full-length SphK-1 (1155 bp) (Gene ID-8877) was amplified using the
207 following primers:

208 NheI_FP: 5′-AATGCTAGCATGGATCCAGCGGGCGGCCCC-3′ and

209 XhoI_RP: 5′-TGGCTCGAGCTATAAGGGCTCTTCTGGCGGTG-3′.

210 The amplified DNA fragment was cloned between NheI and XhoI restriction sites of the pET-
211 28a (+) expression vector, and the recombinant plasmid was transformed into *E. coli* strain
212 BL21 (ʎDE3) gold. The *rhSphK1* protein was eluted after addition of 100mM, 250mM and
213 500mM imidazole solution **(Fig S2B).** Overexpression of 6×His-SphK-1 (*rSphK-1*) was
214 induced with 1mM IPTG (Sigma-Aldrich) at an optical density (OD600) of 0.6, for 4 h at 37°C.
215 The protein was purified using Ni-NTA agarose resin (Qiagen). Briefly, bacterial cells (Rosetta
216 host strains DE3 competent cells (Derivatives of BL21) (Rossetta *E. coli* were obtained from
217 Sigma-Aldrich, USA with catalog number 71397) were used to enhance the production of
218 *rh*SphK-1 by using codons that are infrequently used in *E. Coli*) were harvested (6000 × g for
219 15 min) and lysed by sonication in a lysis buffer containing 50mM Na_2HPO_4 (pH 7.4) and
220 200mM NaCl, supplemented with 500µg/mL Lysozyme (Sigma-Aldrich), and 1mM
221 Phenylmethylsulfonyl Fluoride (PMSF; ThermoFisher Scientific). The bacterial lysate was
222 centrifuged at 10,000 × g for 20 min, and the supernatant obtained was loaded onto a Nickel-
223 Nitrilotriacetic Acid (Ni-NTA) agarose resin (Qiagen)-packed column along with 10 mM
224 imidazole, for 4h at 4°C with mild agitation. The protein was eluted with a continuous
225 imidazole gradient of 25mM, 50mM, 100mM, 250mM, and 500mM. The protein purification
226 was validated by 12% SDS-PAGE, followed by immunoblotting with anti-His tag antibody

227 **(Fig S2B)** (raised in Swiss mice (obtained from the Central Laboratory Animal Resources,
228 Jawaharlal Nehru University, New Delhi) using standard protocol approved by IAEC, JNU).

229 ***Microscale thermophoresis (MST)***

230 To validate the biophysical interaction between *rLd*SphK1 or *rHuman* SphK1 with PF-543 and
231 analyze the binding and kinetics, Microscale Thermophoresis (MST) was performed in
232 NanoTemper Monolith NT.115 instrument. Briefly, 20µM of *rLd*SphK1 or *rHuman* SphK1 in
233 HEPES-NaCl buffer, pH 7.4 was labeled with 30µM Lysine reactive dye (5ul diluted in 200ul
234 *rLd*SphK1 or *rHuman* SphK1 protein) using NanoTemper's Protein Labelling Kit RED-NHS
235 (L001, NanoTemper technologies, Germany) and incubated in the dark for 30 minutes at RT.
236 Following incubation, the labelled *rLd*SphK1 or *rHuman* SphK1 protein along with the buffer
237 was passed through an equilibrated column (provided in the kit). Fractions of the labelled
238 protein were eluted followed by fluorescence count. Fluorescence counts ranging between 250-
239 450 were taken. 5µM PF-543, diluted in HEPES/0.05% Tween-20, was titrated against the
240 constant concentration of the labelled *rLd*SphK1 or *rHuman* SphK1 protein. Pre-mixed
241 samples were incubated for 15 minutes before centrifugation at 8000 rpm for 10 minutes. The
242 samples were filled into the capillaries treated with standards (K002 Monolith NT.115) and
243 thermophoretic mobility was determined. All experiments were performed at RT, at 40% MST
244 power and 20% LED power. Data evaluation was performed with the Monolith software (Nano
245 Temper, Munich, German).

246 ***Biochemical Characterization of Purified rLdSphK and rHumanSphK***

247 The inhibition of *rLd*SphK1 catalytic activity was evaluated in a dose dependent manner with
248 PF-543's concentration ranging from 1 to 5µM. To evaluate the inhibitory effect of PF-543 on
249 the enzymatic activity of *rLd*SphK-1, the protein was pre-incubated with different
250 concentrations of PF-543 (0 to 5µM) for 45 min., followed by initiating the reaction in a buffer

251 containing 0.05% Triton X-100, 1mM ATP, 2% DMSO and NBD-Sph (10μM). The
252 fluorescence intensity of NBD-S1P was measured as described above. The results represented
253 a maximum inhibition at 5μM of PF-543, while the protein concentration was kept constant at
254 200ng.

255 To detect K_m and V_{max} values, varying concentration of NBD Sphingosine (2-20μM) was taken
256 along with 200ng of r*Ld*SphK1. For this, the recombinant protein was incubated with 200μM
257 ATP, NBD–Sphingosine (NBD-Sph) was used as a substrate and conversion of NBD-Sph to
258 NBD-S1P was evaluated. Readings were taken real-time after every 5 sec for 15-20 min at an
259 excitation/emission wavelength of 490/530 nm. Standard curve of SIP was plotted. The
260 enzymatic activities were calculated by plotting fluorescence/time vs substrate concentration
261 followed by plotting of fluorescence/pmoles (velocity) vs substrate concentration. Finally
262 1/Vmax vs 1/[S] was plotted to calculate Km and Vmax according to Lineweaver-Burk plots
263 at 37°C (Lineweaver and Burk, Science Direct, 2011).

264 ***Leishmania cell culture***

265 *Leishmania donovani Bob* promastigotes (*Ld*Bob strain/MHOM/SD/62/1SCL2D, originally
266 obtained from Dr Stephen Beverley (Washington University, St. Louis, MO) were cultured at
267 26°C in M199 medium (Sigma-Aldrich, USA), supplemented with 100 units/ml penicillin
268 (Sigma-Aldrich, USA), 100 μg/ml streptomycin (Sigma-Aldrich, USA) and 10% heat-
269 inactivated fetal bovine serum (FBS; Biowest). Whole cell lysate of promastigote was prepared
270 by freeze–thaw cycles as described previously [41].

271 For axenic amastigotes, the axenically cultured forms grew optimally at a temperature of 32-
272 33°C in a growth media with pH of 5.4. The axenic amastigotes were prepared according to
273 the standard protocol. Briefly, the late-log promastigotes were adapted in an acidic media

274 (RPMI-1640/25 mM 2-(N-morpholino) ethane sulfonic acid (MES)/pH 5.5), at 26°C. These
275 parasites were then grown in RPMI-1640/MES/pH 5.5 at 37°C with 5% CO2.

276 ***Stable transfection of the parasite Leishmania***

277 *Leishmania donovani* Bob strain (*Ld*Bob strain/MHOM/SD/62/1SCL2D) promastigotes were
278 transfected with pXG-GFP-Sphka OE plasmid which harboured the neomycin resistance
279 cassette using electroporation technique as described previously [42] with a Bio-Rad Gene
280 Pulser device and cultured at 26°C in M199 medium (Gibco, Thermofisher scientific USA),
281 supplemented with 100 units/ml penicillin (Sigma-Aldrich, USA), 100 µg/ml streptomycin
282 (Sigma-Aldrich, USA) and 10% heat-inactivated fetal bovine serum (FBS; Gibco, USA). A
283 final concentration of 250 µg/mL of G418 (Sigma-Aldrich, USA) was used to select transfected
284 parasites.

285 ***THP-1 cell culture and infection***

286 THP-1 cells, an acute monocytic leukaemia-derived human cell line (202 TM; American Type
287 Culture Collection, Rockville, MD), were maintained in RPMI-1640 (Sigma-Aldrich, USA)
288 medium supplemented with 10% heat-inactivated FBS (Biowest, UK), 100 units/ml penicillin
289 and 100 µg/ml streptomycin at 37°C and 5% CO_2. Cells (10^6 cells/well) were treated with 50
290 ng/ml phorbol-12-myristate-13-acetate (PMA) (Sigma-Aldrich, USA) for 48h to induce
291 differentiation into macrophage-like-cells before infection. Cells were washed once with
292 phosphate-buffered saline (PBS) and incubated in RPMI medium (Sigma-Aldrich, USA), 10%
293 heat-inactivated FBS, 100 units/ml penicillin and 100 µg/ml streptomycin, before infection. To
294 carry out *in vitro* infection assays, late stationary phase promastigotes (WT) were used at a
295 ratio of 20 parasites per macrophage. *Leishmania*-infected macrophages were incubated at
296 37°C in a 5% CO_2-air atmosphere for 4h to allow the establishment of infection and
297 proliferation of intra-macrophage parasites. The cells were then washed five times with PBS

298 to remove non-adherent extracellular parasites. After that, the cells were incubated in RPMI
299 medium at 37°C in a 5% CO_2-air atmosphere for 48h.

300 ***Infectivity assay***

301 THP-1 cells (1×10^6 cells/well), treated with 50 ng/ml of PMA (Sigma-Aldrich, USA) were
302 seeded on glass coverslips in 6-well plates for 48h. They were infected and simultaneously
303 treated with inhibitors as described above, and the intracellular parasite load (mean number of
304 amastigotes per macrophage) was visualized by Giemsa staining as described previously by
305 Pawar *et al* [43] and expressed as a percentage of the blank controls without drug. At least 10
306 fields were counted manually for each condition to determine the average number of parasites
307 per macrophage.

308 ***qRT-PCR for gene expression analysis***

309 Total RNA from infected macrophages was isolated using the TRIZOL reagent (Sigma-
310 Aldrich, USA) and its concentration was determined by Nanodrop (Thermo Fischer, USA).
311 cDNA was prepared from one microgram of RNase-free DNase treated total RNA using first-
312 strand cDNA Synthesis Kit (Thermo Fischer Scientific, USA), as per manufacturer's
313 instructions, using random hexamer primers. The resulting cDNA was analyzed by quantitative
314 real-time (qRT-PCR) RT-PCR (Applied Biosystems, 7500 Fast Real-Time PCR System, CA,
315 USA) with gene-specific primers using PowerUp SYBR Green PCR Master Mix (Thermo
316 Fisher Scientific, USA). The details of the primers (sequences and annealing temperatures) are
317 given in **Table S1.** Thermal profile for the real-time PCR was amplification at 50°C for 2 min
318 followed by 40 cycles at 95°C for 15 sec, 60°C for 1 min and 72°C for 20 sec. Melting curves
319 were generated along with the mean C_T values and confirmed the generation of a specific PCR
320 product. Amplification of RNU6AP (RNA, U6 small nuclear 1; THP-1 cells) was used as
321 internal control for normalization. The results were expressed as fold change of control

322 (Uninfected samples (RNU6AP)) using the $2^{-\Delta\Delta CT}$method. All samples were run in triplicates,
323 including a no-template (negative) control for all primers used.

324 ***Western blotting***

325 Western blot analysis was done as described previously by Darlyuk et al., 2009 [44]. Briefly,
326 protein was isolated from *Leishmania* infected macrophages by resuspending cell lysates in
327 RIPA buffer. Before lysis, adherent cells were placed on ice and washed with PBS.
328 Macrophages were scraped in the presence of RIPA lysis buffer containing 1% NP-40, 50 mM
329 Tris-HCl (pH 7.5), 150 mM NaCl, 1 mM EDTA (pH 8), 10 mM 1,10-phenanthroline and
330 phosphatase and protease inhibitors (Roche). After incubation, lysates were centrifuged for 15
331 min to remove insoluble matter.The proteins in the lysates were quantified, 80µg of the lysate
332 was boiled (95˚C) for 5 min in SDS sample buffer and was subjected to electrophoresis on a
333 10% SDS-polyacrylamide gel. Proteins were then transferred onto nitrocellulose (NC)
334 membrane using an electrophoretic transfer cell (Bio-Rad Laboratories, USA) at RT. The
335 membrane was washed with 1× TBST solution three times and blocked with 5% BSA for 2h
336 at RT. The blocked membrane was washed in TBST solution three times. The membrane was
337 then incubated with primary monoclonal antibody Caspase 9 (NBP1-69235) in PBS-Tween 20
338 containing 5% BSA and incubated overnight at 4ºC. The blots were subsequently incubated
339 with the secondary antibody conjugated to horseradish peroxidase at 1:3000 dilution in 5%
340 PBS-Tween 20 for 2h at RT. Enhanced chemiluminescence reaction was used for the detection
341 of the blot. The results were expressed as fold change and quantitated by using AlphaEaseFC
342 image analysis software (Alpha Innotech). The data were expressed as mean ± SD of three
343 independent experiments, and the representative image of one experiment is shown.

344 ***Localization of LdSphK1 in L. donovani promastigotes***

345 For detection of SphK1 localization in parasites, $5*10^6$ log phase *Leishmania donovani*
346 promastigotes were plated on poly-L-Lysine coated glass coverslips followed by treatment with

347 500nM PF-543 diluted in incomplete M199 medium for 6h at 22°C in dark. After 6h of
348 treatment, the cells were washed with 1XPBS, fixed (PBS, 4% formaldehyde, 30 min) and
349 permeabilized (PBS, 0.5% Triton X-100, 5 min). Slides were blocked (1% BSA, 1XPBS,
350 overnight at 4°C or for 30 minutes on rocker, RT). Next day blocked cells were incubated with
351 mice raised anti-SphK1 primary antibody (1:500) for 2 hours at RT. The cells were then
352 washed three times with blocking buffer followed by incubation with Alexa 488 conjugated
353 secondary antibody for 1 hour at RT. The coverslips were mounted on glass slides with antifade
354 DAPI solution for visualization under a confocal laser scanning microscope (Olympus
355 FluoViewTM FV1000 with objective lenses PLAPON ×60 O, NA-1.42) at an excitation
356 wavelength of 556 nm. Images were processed via NIS-Elements software version 4.50. The
357 mean fluorescence intensities were plotted using GraphPad Prism version 8.0. The experiment
358 was performed thrice.

359 ***NBD-Sph assay***

360 A fluorescent molecule: omega (7-nitro-2–1, 3-benzoxadiazol-4-yl [2S,3R,4E]-2-amino
361 octadec-4-ene-1,3-diol [NBD–Sphingosine (NBD-Sph); Avanti Polar Lipids]) was used as a
362 substrate and conversion of NBD-Sph to NBD-S1P was evaluated where SIP was estimated as
363 the end metabolite of the sphingolipid metabolism. Towards this, *rLd*SphK1 protein was
364 incubated with 10µM NBD-Sph, at 37°C for 60 min. After incubation, the recombinant protein
365 was lysed with RIPA lysis buffer to obtain host-free protein. The recombinant protein was
366 thoroughly mixed with 260µL of methanol and 400µL of chloroform:methanol (1:1) followed
367 by adding 16µL of 7 M NH4OH, 400µL of chloroform, and 300µL of 1.5 M KCl. The lipids
368 were separated by centrifugation at 17,000 × g for 5 min. A 100µL aliquot of the upper
369 (aqueous) phase was transferred to a black 96-well flat-bottom plate (Corning). Fluorescence
370 intensity of the aqueous phase containing NBD-S1P, in *rLd*SphK1 protein sample was
371 measured at an excitation/emission wavelength of 485 nm/530 nm using Varioskan LUX

372 Multimode Microplate Reader (ThermoFisher Scientific). The fluorescence intensity of NBD-
373 S1P was measured.

374 ***Checkerboard assay***

375 Checkerboard assays were put to evaluate the effects of the combination of Amphotericin-B
376 (anti-fungal agent) and PF-543 (Sphingosine kinase inhibitor) against the *Leishmania* parasite.
377 For this, log-stage promastigotes (42–44h) maintained in M199 media were dispensed in a 96-
378 well plate. Amphotericin-B was added vertically at different concentration ranges while PF-
379 543 was added horizontally at different drug concentration ranges in 8*8 format. As a result,
380 the checkerboard consists of columns and rows in which each of the well along the x-axis
381 contains drug Amphotericin-B at different concentrations (12.5nM, 30nM, 50nM and 100nM)
382 and that along the y-axis contains PF-543 at different concentrations (150nM, 250nM, 500nM
383 and 2μM). The plate was incubated at 25°C in a humidified chamber for 48h. The fractional
384 inhibitory concentration (FIC index = FIC A + FIC B, where FIC A is the IC_{50} of drug (A) in
385 combination/IC_{50} of drug A alone, and FIC B is the IC_{50} of drug B in combination/IC_{50} of drug
386 B alone) of each drug was calculated and plotted as an isobologram. A straight diagonal line
387 with an FIC index equal to 1 indicates an additive effect between drug A and drug B, a concave
388 graph below the diagonal with an FIC index of less than 1 indicates a synergistic effect, and a
389 convex curve above the diagonal with an FIC index of more than 0 indicates antagonism [45-
390 47].

391 ***Estimation of reduced (GSH) and oxidized (GSSG) glutathione levels***

392 The estimation of glutathione levels in reduced and oxidized forms was performed in
393 accordance with the previously documented protocol [48]. Briefly, *Leishmania* infected
394 macrophages were incubated with varying concentrations of SphK inhibitors for 24h and lysate
395 was prepared. For GSH estimation, the lysate was added to an assay mixture containing 0.1

396 mM sodium phosphate buffer (pH 8) and o-phthalaldehyde (1 mg/ml in methanol, Sigma
397 Aldrich, USA) and incubated at RT for 15 min. GSH level was estimated by monitoring
398 fluorescence change at 365Exc/430Emi using a microplate reader. GSSG was also estimated
399 using the same method, however, the lysate was incubated first with N-ethylmaleimide (Sigma
400 Aldrich, USA) in the dark for 5 min, to block the GSH to GSSG oxidation. Results plotted as
401 redox index (GSH/GSSG) ratio are the mean of three independent experiments.

402 ***Animal Studies***

403 Swiss mice were housed under standard conditions of food, temperature (25 ± 3 °C), relative
404 humidity (55 ± 10%) and illumination (12h light/dark cycles) obtained from the Central
405 Laboratory Animal Resources, Jawaharlal Nehru University, Delhi.
406 For experimental assays, infected mice were divided into 4 groups, each group comprise of 3
407 mice. The uninfected group of mice was used as an experimental negative control. The
408 experimental group of mice were infected with *L. donovani* 24h prior to injection with 10
409 mg/kg PF-543 and 2mg/kg amphotericin B alone via I.P route for 3 consecutive days at a dose
410 of body weight, as a Control. While evaluating the synergistic formulation, comprising 2mg/kg
411 PF-543 and 0.4mg/kg amphotericin B, another set of experimental mice were treated once per
412 day for three consecutive days. Evaluation of the immunomodulatory potential was done using
413 cytokine profiling in *Leishmania* infected Swiss mice treated with PF-543 and Amphotericin-
414 B alone and simultaneously followed by determination of parasite infectivity using *in-vitro*
415 parameters. To evaluate the parasitemia and expression of inflammatory markers in infected
416 mice upon drug administration, spleen was harvested from each group of mice and qRT-PCR
417 analysis was performed using primers specific for inflammatory markers; TNF-α and IL-10
418 and parasite specific kinetoplast minicircle gene; JW in PF-543 and Amphotericin-B treated
419 infected mice in respect to the untreated Swiss mice.

420 ***Ethics statement***

421 Animal studies were performed following CPCSEA guidelines and approved by the
422 Institutional Animal Ethics Committee (IEAC) of JNU. Swiss mice were obtained from the
423 Central Laboratory Animal Resources, JNU, New Delhi, and maintained under standard
424 conditions.

425 ***Statistical analysis***

426 Fold-expression (qRT-PCR and densitometric analysis), NBD-Sph and intracellular parasite
427 burden were represented as mean ±SD. Each experiment was repeated three times in separate
428 sets. Statistical differences were determined using Student's unpaired 2-tailed *t*-test. All
429 statistics were performed using GraphPad Prism Version 5.0 (GraphPad Software, USA). $p \leq$
430 0.05 was considered significant [* ($P<0.01$ to 0.05), ** ($P< 0.001$), *** ($P< 0.0001$), ns ($P\geq$
431 0.05)].

432

433 **Results**

434 **1. Expression and Purification of the recombinant *Leishmania* SphK1 (*rLdSphK1*) protein**
435 **and its Functional Characterization in presence and absence of SphK1 inhibitor- PF-543**

436 Detection of *Leishmania*-specific Sphk-1 (*Ld*SphK-1) activity in promastigotes was evaluated
437 using generic inhibitors of SphK; 500nM PF-543, 500µM DMS and 100µM SKI-5C (IC_{50}; **Fig**
438 **4, Fig S3 (A,B)**) for 48h. To investigate the impact of SphK inhibitors; such as PF-543, DMS
439 and SKI-5C on catalytic activity of SphK1 expressed by *Leishmania* promastigotes (*Ld*SphK1),
440 we performed fluorometric assay based estimation of enzymatic activity using 7-nitro-2-1,3-
441 benzoxadiazol-4-yl (NBD)-tagged sphingosine (NBD-sphingosine). The results demonstrated
442 significant reduction of NBD-S1P levels in PF-543-treated *Leishmania* promastigotes, in
443 comparison to untreated control **(Fig 1A),** validating the active catalytic form of the *Ld*SphK1.

444

445 Next, *Ld*Sphk1 was successfully cloned in pET-28 a(+) vector with N-terminal 6x-Histidine-
446 tag **(Fig S1B)** and recombinant protein was purified using affinity based purification method
447 **(Fig S1C)**. For this, we went for expression and purification of the recombinant *Ld*SphK1
448 (*rLd*SphK1) protein and observed a single band corresponding to ~102 kDa on SDS PAGE
449 **(Fig 1B(i))** corresponding to *Leishmania* specific SphK1. Further, the subcellular localization
450 of *rLd*SphK1 was investigated in *L. donovani* Bob cells using confocal microscopy for
451 validation of in-house generated *rLd*SphK1 antibody. Immunostaining of *L. donovani* using
452 anti-*Ld*SphK1 antibody suggested cytoplasmic or membranous localization of *rLd*SphK1 **(Fig**
453 **1B(ii)).**
454 Furthermore, we conducted computational docking analyses of the *Ld*SphK1 protein with the
455 PF-543. The optimal conformations of the docked compounds were chosen based on their
456 minimum free binding energy to the binding domain. Upon analysis of this pocket, it was
457 discovered that there is a single hydrogen bond between residue ARG589 and ligand, with a
458 distance of 2.03 Å. In addition, GLU586, ARG591, ARG596, LEU632, and ASP636
459 established hydrophobic contacts within the pocket. The binding of PF-543 to the protein is
460 facilitated by these interactions, which result in a minimum binding energy of -7.93 kcal/mol
461 **(Fig 1C)**. The analysis of these results indicates that PF-543 creates a stable structure when
462 bound to the *Ld*SphK1 binding pocket. These data inferred that *rLdSphK1* and PF-543 are
463 possible interacting partners having favourable binding energy.
464 To validate the biophysical interaction between purified *rLd*SphK1 and PF-543 and analyze
465 the binding and kinetics, Microscale Thermophoresis (MST) was performed in NanoTemper
466 Monolith NT.115 instrument. Herein, labelled *rLdSphK1* (20µM) was titrated against varying
467 concentrations of PF-543 (500nM, 1µM, 2.5µM, 5µM, 10µM, 20µM). The dose response
468 analysis for *rLdSphK1*-PF-543 binding revealed dissociation constant, K_D to be 29.3µM,
469 suggesting strong binding of *rLdSphK1* with PF-543 **(Fig 1D).** Additionally, we also evaluated

470 interaction between *rLdSphK1* and ABC294640 as a negative experimental control where no
471 such binding between the two could be detected.
472 The time course kinetics for *rLdSphK1* was done using NBD-Sphingosine based fluorometric
473 assay for detection of NBD-S1P levels. The results represented a steep increment in NBD-S1P
474 level with *rLdSphK1* concentration ranging from 200ng to 500ng **(Fig 1E(i)),** following which
475 saturation in activity was detected (data not shown). In addition, the inhibition of *rLd*SphK1
476 catalytic activity was also evaluated in a dose dependent manner with PF-543's concentration
477 ranging from 1 to 5µM. The results represented a maximum inhibition at 5µM of PF-543, while
478 the protein concentration was kept constant at 200ng **(Fig 1E(ii)).** To detect Km and Vmax
479 values, varying concentration of NBD Sphingosine (2-10µM) was taken along with 200 ng of
480 *rLd*SphK1. The results confirmed 48.17µM and 114.5µM as Km and Vmax respectively,
481 according to Lineweaver-Burk plots, while D-erythro-sphingosine is used as the substrate for
482 *Ld*SphK1 **(Fig 1E(iii)).**
483
484 **2. Expression and Purification of the recombinant Human SphK1 (*rhSphK1*) protein and**
485 **its Functional Characterization in presence and absence of SphK1 inhibitor- PF-543**
486 Initially, we conducted the amino acid sequence alignment of LD_SphK1 and Human_SphK1
487 utilizing MEGAX program (version 10.2.2). It demonstrated considerable alignment with
488 similar and a limited number of identical amino acids **(Fig S4A)**. Additionally, we conducted
489 3D structural alignment of the two protein structures with Pymol software. We observed
490 substantial alignment between the two proteins, with an RMSD of 0.585. Furthermore, the
491 alpha helix and beta sheets of the Human DAGKc domain (Blue) are accurately aligned with
492 the LD_DAGKc domain (Yellow) in **(Fig S4B)**. A phylogenetic tree was created utilizing
493 SPHK1 gene sequences from various species of *Leishmania*, humans, rats, and mice. The
494 phylogenetic tree was constructed using neighbor-joining technique with MEGAX software.

495 Bootstrap analyses with 1000 replicates were conducted to evaluate the robustness of the
496 constructed phylogenetic tree **(Fig S4C)**.
497 Next, *Human*Sphk1 was successfully cloned in pET-28 a(+) expression vector, and the
498 recombinant plasmid was transformed into *E. coli* strain BL21 (λDE3) gold**.** Later, we went
499 for expression and purification of the recombinant *Human*SphK1 (*rHuman*SphK1) protein **(Fig**
500 **S2B).** A single band corresponding to ~50 kDa was observed on SDS PAGE **(Fig 2A)**
501 corresponding to Human specific SphK1.
502 In order to assess the underlying physiological mechanisms of protein-ligand interactions, we
503 conducted *in-silico* docking experiments involving the hSphK1 protein and the PF-543
504 compound. The optimal conformations of the docked compounds were chosen based on their
505 minimum free binding energy to the binding domain. Upon examination of this pocket, it was
506 discovered that it contains two residues, namely HIS156 and THR157, which are linked
507 together by hydrogen bonds. The hydrogen link between them has a distance of 3.44 Å, while
508 the other hydrogen bond has a distance of 2.53 Å. Similarly, GLU93, LEU161, VAL227,
509 GLN230, GLN231, and PRO240 established hydrophobic interactions within the pocket. The
510 binding of PF-543 to the protein is facilitated by these interactions, resulting in a minimum
511 binding energy of -8.59 kcal/mol **(Fig 2B).** The analysis of these results indicates that PF-543
512 creates a stable structure when bound to the hSphK1 binding pocket. These data inferred that
513 *rhSphK1* and PF-543 are possible interacting partners having favourable binding energy.
514 To validate the biophysical interaction between purified *rhSphK1* and PF-543, MST was
515 performed in NanoTemper Monolith NT.115 instrument. Herein, labeled *rhSphK1* (20μM) was
516 titrated against varying concentrations of PF-543. The dose response analysis for binding
517 between *rhSphK1*-PF-543 and *rhSphK1*-ABC294640 (SphK2 inhibitor) revealed dissociation
518 constant, K_D to be 34.3μM, and 70.6μM respectively suggesting strong binding of *rhSphK1*
519 with PF-543 and ABC294640 respectively **(Fig 2C).**

520 Further, the time course kinetics for *rhSphK1* was done using NBD-Sphingosine based
521 fluorometric assay for evaluating its functional active form. The results represented a steep
522 increment in generation of NBD-S1P level with 200 ng *rhSphK1* **(Fig 2D (i)),** following which
523 saturation in activity was detected (data not shown). To detect Km and Vmax values, varying
524 concentration of NBD Sphingosine (2-10µM) was taken along with 200ng of *rhSphK1*. The
525 results confirmed 62.98µM and 152.4µM as Km and Vmax respectively with D-erythro-
526 sphingosine is used as the substrate for *rhSphK1* **(Fig 2D (ii)).**
527
528 **3. Effect of PF-543 on cytotoxicity and infectivity of *L. donovani* SphK1 overexpressor**
529 ***(Ld*SphKa) promastigotes**
530 To confirm successful transfection of *Leishmania donovani* promastigotes with the pXG-GFP-
531 SphKa construct, parasites were examined under confocal microscopy for GFP expression. A
532 distinct population of GFP-positive parasites was detected, confirming transgene expression,
533 alongside a subset of GFP-negative cells **(Fig 3A).** Non-transfected GFP-tagged parasites were
534 included as controls to validate the specificity of transgene expression.
535 Detection of *Leishmania*-specific Sphk-1 (*Ld*SphK-1) activity in *Leishmania* SphK1 over-
536 expressor promastigotes was detected using generic inhibitors of SphK. To investigate the
537 impact of SphK inhibitors; such as PF-543, DMS and SKI-5C on catalytic activity of SphK1
538 expressed by *Leishmania* over-expressor promastigotes (*Ld*SphKa), we performed
539 fluorometric assay based estimation of enzymatic activity using 7-nitro-2-1,3-benzoxadiazol-
540 4-yl (NBD)-tagged sphingosine (NBD-sphingosine). The results demonstrated higher but
541 similar levels of NBD-S1P in PF-543, DMS and SKI5C-treated *Ld*SphKa promastigotes, in
542 comparison to untreated control **(Fig 3B (i)),** validating the overexpression of active catalytic
543 form of the SphK1 in *Leishmania donovani.*

544 Subsequently, the cytotoxic effect of PF-543 on *Leishmania* SphK1-overexpressing
545 promastigotes was assessed using the MTT assay. PF-543 exhibited cytotoxicity against
546 *Ld*SphKa promastigotes with an IC_{50} value of 42.71μM, notably higher than that observed for
547 wild-type *L. donovani* promastigotes **(Fig 3B (ii)).** These results suggest that overexpression
548 of SphK1 may confer partial resistance to PF-543-induced cytotoxicity, potentially by
549 modulating downstream lipid signaling pathways.
550 To evaluate the impact of SphK1 over-expression on clearance of intracellular load of
551 amastigotes, THP-1 cells were infected with *Ld*SphKa promastigotes at various MOIs (10:1,
552 20:1, 30:1, 50:1). The intracellular parasite burden was analysed using RT-PCR at 48h post-
553 infection. Uninfected (UI)THP-1 cells were used as experimental controls. At an MOI of 10:1,
554 approximately 86% infection was observed in *Ld*SphKa-infected THP-1 cells, indicating
555 efficient parasite entry and survival. In comparison, *Bob*-infected THP-1 cells demonstrated
556 ~80% infection at an MOI of 20:1 **(Fig 3C).** Across higher MOIs (20:1, 30:1, and 50:1),
557 infection rates remained consistently higher in the *Ld*SphKa group relative to the *Bob*-infected
558 controls **(Fig 3C),** confirming that SphK1 overexpression is associated with enhanced
559 infectivity and a rapid-growth phenotype.
560 These findings collectively suggest that SphK1 plays a crucial role in promoting parasite
561 survival and proliferation, and that its overexpression may attenuate the antiparasitic effects of
562 PF-543.
563
564 **4. Cytotoxicity and infectivity of *L. donovani* upon PF-543 treatment**
565 The cytotoxic effect of PF-543 was studied in both THP-1 macrophages; an acute monocytic
566 leukaemia-derived human cell line (202 TM; American Type Culture Collection, Rockville,
567 MD) and *Leishmania* spp (*Ld*Bob strain/MHOM/SD/62/1SCL2D) promastigotes using MTT
568 assay. The selectivity index (SI) representing the ratio of cytotoxicity in THP-1/promastigotes

569 (CC_{50}/IC_{50}) was determined for PF-543 treatment. The results demonstrated PF-543 to be more
570 toxic to the intracellular parasites than to the host cells. The IC_{50} of PF-543 was 90µM for THP-
571 1 macrophages, 17.54µM for intracellular amastigotes and 45µM for axenic amastigotes
572 respectively, as determined by cytotoxic or metabolic viability analysis. These findings are
573 summarized in **Fig 4** that provided information on the Inhibitory Concentrations (IC_{50}). The
574 data analysis showed PF-543 had an IC_{50} of 500nM and SI of 180nM **(Fig 4A).** In contrast,
575 ABC294640 was found to be toxic to host cells expressing the SphK2 isoform, with IC_{50} values
576 of 60µM for THP-1 macrophages and 69.7µM for intracellular amastigotes **(Figure S3C).**
577 To evaluate the impact of PF-543 on clearance of intracellular load of amastigotes, THP-1 cells
578 were treated with PF-543 (90µM) prior to infection with *L. donovani* at an MOI of 20:1. The
579 intracellular parasite burden was analyzed using RT-PCR and Giemsa staining at 48h post-
580 infection. On analysis, Untreated- uninfected (UT-*Ld*) THP-1 cells were used as experimental
581 controls and could able to show ~ 80% infection with *L. donovani*. While PF-543 treated THP-
582 1 (24h post-treatment) showed ~ 60% of infection **(Fig 4B (i,ii)).** Upon comparing the clearance
583 of parasitic load in PF-543 treated infected THP-1 cells (PF543+*Ld*) with untreated infected
584 THP-1 (UN+*Ld*), ~40% reduction in the number of parasites (amastigotes/macrophage) was
585 detected per infected macrophage **(Fig 4B (i,ii)).**
586 These findings suggest that inhibition of host SphK1 via PF-543 significantly reduces
587 intracellular parasite load, likely by impairing the parasite's ability to sustain its intracellular
588 growth. This points to a persistent, slow-growth phenotype of parasites exposed to SphK1
589 inhibition.
590

591 **5. Decrease in *Leishmania* glutathione levels mediates ceramide-induced parasite death**

592 *Leishmania* infection leads to increase in ceramide generation that further depletes cholesterol
593 from the membrane and disrupts lipid rafts resulting in weak CD40 mediated signalling that

594 leads to increased ERK1/2 phosphorylation and impaired antigen presentation to the T cells,
595 worsening the diseased condition [49].
596 DL-threo-PPMP, a ceramide analog is known to inhibit the activity of glucosylceramide
597 synthase. Here in this study, it was used to investigate the role of ceramide in *Leishmania*
598 parasite death. Exogenously added ceramide synthase inhibitor, DL-threo-PPMP at
599 concentrations of 20μM exhibited a dose-dependent cytotoxic effect (expressed as growth
600 inhibition) on THP-1 macrophages **(Fig S5).**
601 THP-1 cells were infected with *L. donovani* at an MOI of 20:1 followed by treatment with DL-
602 threo-PPMP. The glutathione and apoptotic levels were analysed using GSSH/GSG assay and
603 Western blot at 48h post-treatment. On analysis, we found that addition of ceramide synthase
604 inhibitor induced a decrease in GSH/GSSG ratio **(Fig 5A)** and an increase in Caspase 9 levels
605 **(Fig 5B)** in *Leishmania* infected macrophages.
606 Sphingosine-1-phosphate (S1P), a metabolite of the sphingomyelin pathway and a biological
607 antagonist of ceramide action, prevents ceramide-induced death in mammalian cells [30]. To
608 determine whether S1P can prevent the killing effect of ceramide, *Leishmania* infected
609 macrophages were exposed to PPMP with or without S1P at 10μM (a non-toxic concentration
610 for the parasites). The cytotoxic effect of ceramide found by observing high Caspase levels was
611 significantly reduced by exogenous addition of S1P **(Fig 5B)** and was also found to restore the
612 levels of GSH/GSSG in SIP supplemented cells **(Fig 5A).** These findings suggest the
613 prevention of ceramide-induced toxicity for leishmania parasites by sphingosine-1-phosphate.
614
615 **6. Elucidation of inflammatory responses and infectivity post-PF-543 treatment in**
616 ***Leishmania* infected macrophages**
617 Cytokines play a crucial role in mediating T-cell responses and host defense mechanisms in
618 macrophages. LPS potently activates macrophages and cytokine signalling by TLR4

619 stimulation, while *Leishmania* parasites suppress LPS-induced host inflammatory cytokine
620 responses [50]. We investigated the effect of perturbation of the host SphK1 pathway on the
621 pro-inflammatory and anti-inflammatory cytokines from LPS-stimulated *Leishmania* infected
622 macrophages. We found that PF-543 post-treatment in infected macrophages reduced the levels
623 of anti-inflammatory cytokine *IL-10* (~80%) as confirmed by RT-PCR and ELISA while the
624 level of pro-inflammatory cytokines *IL32γ*, *IL-12* and *TNF-α* remain unaltered **(Fig 6A (i,ii)).**
625 We further evaluated the parasite load in presence of PF-543 using qRT-PCR based on
626 estimation of JW (kDNA) mRNA levels in PF-543 treated and untreated infected cells. The
627 results suggested PF-543 post-treatment leads to decrease in parasite load in infected
628 macrophages **(Fig 6B),** thereby indicating the role of PF-543 in reducing the parasite survival.
629

630 **7. Evaluation of antileishmanial activity of PF-543 and Amphotericin B combined**
631 **formulation against *L. donovani* promastigotes and intracellular amastigotes**

632 Amphotericin B (Amph-B) is a first-line medication for treating leishmaniasis specifically
633 *Leishmania donovani* infection, in India [51]. Amph-B which binds to the ergosterol of
634 protozoan cells causes a change in membrane integrity resulting in ions leakage, and ultimately
635 leading to cell death [52]. We also checked the potential impact of Amphotericin B the current
636 drug used in clinics, alone and in combination with PF-543 on anti-leishmanial activity against
637 *L. donovani* promastigotes using MTT assay. The *in-vitro* synergistic activity of PF-543 along
638 with Amphotericin B was represented by an isobologram. Upon analysis of antileishmanial
639 activity, Amphotericin B showed an IC_{50} of 30nM and PF-543 showed IC_{50} of 500nM alone
640 **(as already shown in Fig 4A)** however upon administering both PF-543 and Amphotericin B
641 in combination, synergistic impact was prominent, and the IC_{50} was observed to be ~12.5nM
642 and 150nM for Amphotericin B and PF-543 respectively, as depicted by the isobologram
643 micrographs in promastigotes **(Fig 7A).**

644 For validating the anti-leishmanial activity by PF-543 and Amphotericin B formulation on
645 intracellular amastigotes, qPCR-based analysis was performed for all the treatments. Here-in
646 the synergistic treatment of Amphotericin B (12.5nM) and PF-543 (150nM) formulation to
647 intracellular amastigotes reduced the parasite growth by 60%. Whereas, treatment with PF-543
648 or Amphotericin B alone decreased the parasite burden by 30%. Further reduction of 40% and
649 60% in parasite growth was observed with usage of higher dosage of PF-543 alone (250nM,
650 500nM and 2000nM), while these doses in combination with Amphotericin-B (12.5nM +
651 150nM, 12.5nM + 250nM, 12.5nM + 500nM, 12.5nM + 2000nM) showed higher reduction of
652 parasite growth to ~80-90% **(Fig 7B).** These data clearly suggested that PF-543 along with
653 Amphotericin B can be a promising potent formulation to be tested.
654
655 **8. Elucidation of inflammatory responses and infectivity post-PF-543 treatment in**
656 ***Leishmania*-infected Swiss mice**
657 To check the anti-leishmanial activity of PF-543 *in vivo*, the experimental group of mice were
658 infected with *L. donovani* 24h prior to injection with 10mg/kg PF-543 and 2mg/kg
659 amphotericin B alone via I.P route for 3 consecutive days at a dose of body weight, as a Control**.**
660 While evaluating the synergistic formulation, comprising 2mg/kg PF-543 and 0.4mg/kg
661 amphotericin B, another set of experimental mice were treated once per day for three
662 consecutive days. Evaluation of the immunomodulatory potential was done using cytokine
663 profiling in *Leishmania* infected Swiss mice treated with PF-543 and Amphotericin-B alone
664 and simultaneously followed by determination of parasite infectivity using *in-vitro* parameters.
665 To evaluate the parasitemia and expression of inflammatory markers in infected mice upon
666 drug administration, spleen was harvested from each group of mice and qRT-PCR analysis was
667 performed using primers specific for inflammatory markers; *mTNF-α* and *mIL-10* **(Table S1)**

668 and parasite specific kinetoplast minicircle gene; *JW* in PF-543 and Amph-B treated infected
669 mice in respect to the untreated Swiss mice.
670 In concordance with the published studies, here-in, upon analysis, treatments with either
671 Amphotericin B or PF-543 alone in infected mice resulted in a significant decrease in *IL-10*
672 expression, whereas increased *TNF-α* expression was observed **(Fig 8A).** Further, this effect
673 on inflammatory markers was more pronounced upon the synergistic treatment of
674 Amphotericin B and PF-543 formulation to *Leishmania* infected Swiss mice **(Fig 8A).**
675 Most importantly, parasite load was also observed to be reduced upon treatment with PF-543
676 or Amphotericin B alone in infected mice **(Fig 8B)** where ~33% and ~80% reduction in parasite
677 growth was observed respectively. Further, this down-regulation in parasite burden was
678 drastically reduced to >90% (as demarcated by reduction in *JW* transcript) upon synergistic
679 treatment of PF-543 and Amphotericin B formulation **(Fig 8B).**
680

681 **Discussion**

682 The current study elucidates the role of sphingosine kinase 1 (SphK1) in the pathogenesis of
683 *Leishmania donovani* and its potential as a therapeutic target. Our findings demonstrate that
684 inhibition of SphK1 using PF-543, a selective inhibitor, leads to significant disruption in the
685 parasite's survival, proliferation, and host cell interactions. These results align with previous
686 studies that have shown the critical role of SphK1 in various protozoan parasites, suggesting
687 that targeting this enzyme can impair parasite viability [53,54]. Furthermore, the combination
688 of PF-543 with Amphotericin B shows promise as a synergistic treatment strategy, with
689 enhanced efficacy against both promastigotes and intracellular amastigotes. This is consistent
690 with recent reports where drug combinations have been shown to enhance treatment efficacy
691 and reduce resistance [55,56].

692 We successfully cloned and expressed recombinant *Leishmania* SphK1 (*rLd*SphK1) in a
693 prokaryotic system and confirmed its enzymatic activity through fluorometric assays. Similar
694 approaches to express and characterize SphK1 from *Leishmania* and other protozoan parasites
695 have been reported, confirming its vital role in their metabolic pathways [57]. The results
696 indicated that PF-543 inhibited the enzymatic activity of *rLd*SphK1 in a dose-dependent
697 manner, reducing the levels of sphingosine-1-phosphate (S1P), a key signalling molecule that
698 regulates cell growth and survival [58]. Additionally, the subcellular localization of *rLd*SphK1
699 in *Leishmania* promastigotes was primarily cytoplasmic and membranous, aligning with
700 previous reports on SphK1 localization in other organisms [59,60].

701 Computational docking studies revealed that PF-543 binds effectively to the active site of
702 *Ld*SphK1, with favourable binding interactions between key amino acid residues (e.g.,
703 ARG589, GLU586). These findings are supported by similar studies where small-molecule
704 inhibitors have been designed to target the SphK1 enzyme, offering a potential strategy to
705 selectively block SphK1 in parasitic infections [61]. The dissociation constant (K_D) of 29.3µM,
706 measured by Microscale Thermophoresis (MST), confirmed strong binding between PF-543
707 and *rLd*SphK1. These biophysical and computational analyses strengthen the hypothesis that
708 PF-543 directly targets and inhibits SphK1 activity in *Leishmania*. Similar experiments were
709 performed with human SphK1 (*rh*SphK1), and PF-543 exhibited a comparable inhibitory
710 effect, with a slightly weaker binding affinity (K_D = 34.3µM for *rh*SphK1 vs. 70.6µM for
711 SphK2) in MST assays. This suggests that PF-543 could potentially inhibit human SphK1 with
712 similar efficiency, further justifying its consideration for therapeutic use in both parasitic and
713 human diseases.

714 The study extended to *Leishmania* promastigotes with overexpressed SphK1 (*Ld*SphKa). PF-
715 543 treatment showed a higher IC_{50} in these overexpressor parasites, suggesting that increased

716 SphK1 expression might partially confer resistance to the inhibitor. However, even in these
717 overexpressor strains, PF-543 still exhibited a ~40% reduction in parasite load within infected
718 macrophages. This emphasizes the importance of targeting SphK1 in *Leishmania* and suggests
719 that while overexpression may confer partial resistance, inhibition of SphK1 still holds
720 therapeutic potential, as also observed in studies targeting SphK1 in cancer cells [62].

721 The cytotoxic effect of PF-543 was evaluated in both *Leishmania* promastigotes and human
722 THP-1 macrophages. The results indicated that PF-543 had a lower cytotoxic effect on THP-1
723 cells, with an IC_{50} of 90µM, compared to its potent action on *Leishmania* promastigotes and
724 intracellular amastigotes. This selective toxicity aligns with findings previously reported [63],
725 where SphK1 inhibition was shown to preferentially target pathogens without causing
726 significant harm to host cells. The IC_{50} of 500nM highlighted PF-543's preferential toxicity
727 toward the parasite, reinforcing the idea that targeting SphK1 can selectively inhibit parasite
728 growth without major toxicity to host cells.

729 Furthermore, PF-543 treatment led to reduced intracellular parasite burden in THP-1 cells, with
730 a 40% reduction in parasite load, confirming its efficacy in controlling the infection. This result
731 is consistent with similar findings in other studies, where SphK1 inhibitors significantly
732 reduced parasite burden in macrophages infected with *Leishmania* species [64]. This was
733 further supported by RT-PCR analysis showing decreased parasite-specific mRNA levels,
734 indicating that PF-543 effectively reduces parasite survival within host cells.

735 *Leishmania* infection leads to increased ceramide generation, which disrupts membrane
736 integrity and impairs antigen presentation, contributing to the pathogenesis [65]. Our study
737 demonstrated that inhibition of ceramide synthesis using DL-threo-PPMP led to a decrease in
738 parasite viability, as evidenced by increased caspase-9 activity and a decreased GSH/GSSG
739 ratio. Interestingly, exogenous addition of sphingosine-1-phosphate (S1P) reversed the

740 cytotoxic effect of ceramide, suggesting that S1P acts as a protective factor against ceramide-
741 induced parasite death. These findings underscore the complex interplay between sphingolipid
742 metabolism and parasite survival and highlight the potential therapeutic value of modulating
743 this pathway [66].

744 SphK1 is known to play a crucial role in modulating the inflammatory response, and its
745 inhibition has the potential to alter host immune responses. In *Leishmania*-infected
746 macrophages, PF-543 treatment resulted in reducing the levels of the anti-inflammatory
747 cytokine IL-10. This shift towards a pro-inflammatory profile is consistent with the known
748 immunomodulatory effects of sphingosine kinase inhibition [67,68]. This may contribute to
749 enhanced host defense against the infection, as IL-12 and TNF-α are critical for controlling
750 *Leishmania* replication [69]. The decrease in IL-10 expression could help mitigate the immune
751 suppression typically induced by *Leishmania*, which facilitates parasite survival. This suggests
752 that PF-543 not only targets the parasite directly but also modulates the host immune
753 environment to favour parasite clearance.

754 As per previous reports, Amphotericin B, a widely used anti-leishmanial drug, targets the
755 parasitic membrane by binding to ergosterol, but its use is limited due to toxicity and resistance
756 concerns [70]. Our study explored the combination of PF-543 and Amphotericin B, finding a
757 synergistic effect. The IC_{50} values for the combination treatment were significantly lower
758 compared to individual drugs, with a greater than 80% reduction in parasite burden in both
759 promastigotes and intracellular amastigotes. This synergy may be due to PF-543's ability to
760 alter sphingolipid metabolism, affecting membrane integrity and facilitating increased
761 susceptibility to Amphotericin B-induced damage, as demonstrated in previous work by Al-
762 Rawi *et al* [71].

763 Further, *in vivo* studies in *Leishmania*-infected Swiss mice showed that PF-543, either alone or
764 in combination with Amphotericin B, significantly reduced the parasite load in spleen tissues.
765 Treatment with the combination therapy resulted in a >90% reduction in parasite burden,
766 compared to a ~33% reduction with PF-543 alone and ~80% reduction with Amphotericin B
767 alone. Cytokine analysis revealed an increase in TNF-α expression and a decrease in IL-10,
768 further supporting the immune-modulatory role of PF-543 *in vivo*. These findings are consistent
769 with studies showing that combination therapies enhance anti-parasitic efficacy and improve
770 immune responses in *Leishmania*-infected models [72].

771 In conclusion, this study provides compelling evidence for the crucial role of SphK1 in
772 *Leishmania* survival and pathogenesis and highlights the potential of PF-543 as a selective
773 inhibitor. The combination of PF-543 with Amphotericin B shows significant promise as a
774 synergistic treatment strategy against *Leishmania donovani*. Further investigation into the
775 long-term effects and potential clinical applications of this combination therapy is warranted,
776 particularly in the context of combating drug resistance and enhancing immune responses in
777 infected hosts. Additionally, modulating sphingolipid metabolism offers a novel therapeutic
778 approach for leishmaniasis.

779

780 **Competing Interest**

781 The authors declare no competing interests.

782

783 **Acknowledgments**

784 Singh S conceptualized the work, designed the experiments, interpreted the data and edited the
785 manuscript. EM executed the experiments, performed the data interpretation and wrote the
786 manuscript. EM, RB, JS, MS, SS and NJ performed immunological studies, microscopy,

787 molecular assays, parasite culture, cloning, protein purification and mice experiments. This
788 study was funded by CSIR Scientist Pool Officer (SRA) funding agency research grant
789 (13(9160-A)2021-Pool) provided to Dr. Evanka Madan. RB and JS were supported by DHR-
790 Women Scientist and BioCARe Women Scientist from DBT respectively. SS is a recipient of
791 the National Bio Scientist Award. All authors contributed to the article and approved the
792 submitted version. The work in Shailja Singh's lab at Special Centre for Molecular Medicine
793 (SCMM), JNU, is supported by IRHPA IPA/2020/000007, Department of Science and
794 Technology and Drug and Pharmaceuticals Research Program (DPRP) (Project No.
795 P/569/2016-1/TDT, SS). We would like to acknowledge Prof. Md. Imtiyaz Hassan (Professor,
796 Structural Biology Laboratory, Jamia Millia Islamia) for providing us with the Human SphK1
797 clone and Prof. Zhang, Kai (Professor, Department of Biological Sciences, Texas Tech
798 University) for providing us with pXG-GFP-SKa plasmid which we used to overexpress SKa
799 (or SphK1) in *L. donovani*. The funders had no role in the study design; collection, analysis,
800 and interpretation of data; in the writing of the report; and in the decision to submit this article
801 for publication.

802

803 **Plagiarism Check**

804 This manuscript has been screened for plagiarism and found to be original.

805 **References**

806 1. Alvar J, Vélez ID, Bern C, Herrero M, Desjeux P, Cano J, et al. Leishmaniasis worldwide
807 and global estimates of its incidence. PLoS One. 2012;7:e35671.

808 2. Arango Duque G, Descoteaux A. Leishmania survival in the macrophage: Where the ends
809 justify the means. Curr Opin Microbiol. 2015;26:32-40.

810 3. Rub A, Arish M, Husain SA, Ahmed N, Akhter Y. Host-lipidome as a potential target of
811 protozoan parasites. Microbes Infect. 2013;15:649-60.

812 4. Bhargava P, Singh R. Developments in diagnosis and antileishmanial drugs. Interdiscip
813 Perspect Infect Dis. 2012;2012:626838.

814 5. Mahmoudvand H, Sharififar F, Sharifi I, Ezatpour B, Fasihi Harandi M, Makki MS, et al. In
815 vitro inhibitory effect of Berberis vulgaris and its main component, berberine against different
816 Leishmania species. Iran J Parasitol. 2014;9:28-36.
817
818 6. Moore EM, Lockwood DN. Treatment of visceral leishmaniasis. J Glob Infect Dis.
819 2010;2(2):151-8.

820 7. Datta A, Podder I, Das A, Sil A, Das NK. Therapeutic modalities in post kala-azar dermal
821 leishmaniasis: A systematic review of the effectiveness and safety of the treatment options.
822 Indian J Dermatol. 2021;66(1):34-43.

823 8. Huang LS, Berdyshev E, Mathew B, Fu P, Gorshkova IA, He D, et al. Targeting sphingosine
824 kinase 1 attenuates bleomycin-induced pulmonary fibrosis. FASEB J. 2013;27:1749-60.

825 9. Chen J, Tang H, Sysol JR, Moreno-Vinasco L, Shioura KM, Chen T, et al. The sphingosine
826 kinase 1/sphingosine-1-phosphate pathway in pulmonary arterial hypertension. Am J Respir
827 Crit Care Med. 2014;190:1032-43.

828 10. Price MM, Oskeritzian CA, Falanga YT, Harikumar KB, Allegood JC, Alvarez SE, et al.
829 A specific sphingosine kinase 1 inhibitor attenuates airway hyperresponsiveness and
830 inflammation in a mast cell-dependent murine model of allergic asthma. J Allergy Clin
831 Immunol. 2013;131:501-11.e1.

832 11. Wang L, Chen F, Pan Y, Lin L, Xiong X. Effects of FTY720 on lung injury induced by
833 hindlimb ischemia reperfusion in rats. Mediators Inflamm. 2017;2017:5301312.

834 12. Nishiuma T, Nishimura Y, Okada T, Kuramoto E, Kotani Y, Jahangeer S, et al. Inhalation
835 of sphingosine kinase inhibitor attenuates airway inflammation in asthmatic mouse model. Am
836 J Physiol Lung Cell Mol Physiol. 2008;294:L1085-93.

837 13. Arish M, Husein A, Ali R, Tabrez S, Naz F, Ahmad MZ, et al. Sphingosine-1-phosphate
838 signaling in Leishmania donovani infection in macrophages. PLoS Negl Trop Dis.
839 2018;12:e0006360.

840 14. Pulkoski-Gross MJ, Obeid LM. Molecular mechanisms of regulation of sphingosine kinase
841 1. Biochim Biophys Acta Mol Cell Biol Lipids. 2018;1863:1413-22.

842 15. Zhang O, Hsu FF, Xu W, Pawlowic M, Zhang K. Sphingosine kinase A is a pleiotropic and
843 essential enzyme for Leishmania survival and virulence. Mol Microbiol. 2013;90(3):489-501.

844 16. Cao M, Ji C, Zhou Y, Huang W, Ni W, Tong X, et al. Sphingosine kinase inhibitors: A
845 patent review. Int J Mol Med. 2018;41:2450-60.

846 17. Patel DS, Ahmad F, Abu Sneineh M, Patel RS, Reddy SR, Llukmani A, et al. The
847 importance of sphingosine kinase in breast cancer: A potential for breast cancer management.
848 Cureus. 2021;13(2):e13413.

849 18. Kim SB, Limbu KR, Oh YS, Kim SL, Park SK, Baek DJ, et al. Novel dimer derivatives of
850 PF-543 as potential antitumor agents for the treatment of non-small cell lung cancer.
851 Pharmaceutics. 2022;14(2):369.

852 19. Yakhak Hoeji. Antitumor activity of PF-543 and PF-543 derivative (22c) as sphingosine
853 kinase 1 inhibitors. Yakhak Hoeji. 2018;62(5):293-6.

854 20. Sah RK, Anand S, Dar W, Jain R, Kumari G, Madan E, et al. Host-erythrocytic sphingosine-
855 1-phosphate regulates Plasmodium histone deacetylase activity and exhibits epigenetic control
856 over cell death and differentiation. Microbiol Spectr. 2023;11(2):e02766-22.

857 21. Romano PS, Akematsu T, Besteiro S, Bindschedler A, Carruthers VB, Chahine Z, et al.
858 Autophagy in protists and their hosts: When, how and why? Autophagy Reports.
859 2023;2(1):2149211.

860 22. New RR, Chance ML, Heath S. Antileishmanial activity of amphotericin and other
861 antifungal agents entrapped in liposomes. J Antimicrob Chemother. 1981;7(4):371–81.

862 23. Verma J, Verma L, Tripathi K. Sterol enriched mixed lamellarity amphotericin intercalating
863 liposomes in saline and the process for their preparation. US Patent 2007/0218119 A1.

864 24. Aslett M, Aurrecoechea C, Berriman M, Brestelli J, Brunk BP, Carrington M, et al.
865 TriTrypDB: a functional genomic resource for the Trypanosomatidae. Nucleic Acids Res
866 [Internet]. 2010 [cited 2023 Dec 21];38(Database issue):D457–62.

867 25. Troshin PV, Procter JB, Barton GJ. Java bioinformatics analysis web services for multiple
868 sequence alignment—JABAWS:MSA. Bioinformatics. 2011;27(14):2001–2.

869 26. Kumar S, Stecher G, Li M, Knyaz C, Tamura K. MEGA X: Molecular evolutionary
870 genetics analysis across computing platforms. Mol Biol Evol. 2018;35(6):1547–9.

871 27. DeLano WL. PyMOL: An open-source molecular graphics tool. CCP4 Newsl Protein
872 Crystallogr [Internet]. 2002;40:82–92.

873 28. Berman HM. The Protein Data Bank. Nucleic Acids Res. 2000;28(1):235–42.

874 29. The UniProt Consortium. UniProt: a hub for protein information. Nucleic Acids Res.
875 2015;43(Database issue):D204–12.

876 30. Ivens AC, Peacock CS, Worthey EA, Murphy L, Aggarwal G, Berriman M, et al. The
877 genome of the kinetoplastid parasite, Leishmania major. Science. 2005;309(5733):436–42.

878 31. Kelley LA, Mezulis S, Yates CM, Wass MN, Sternberg MJ. The Phyre2 web portal for
879 protein modeling, prediction and analysis. Nat Protoc [Internet]. 2015 [cited 2021 Aug
880 7];10(6):845–58. Available from: https://www.nature.com/articles/nprot.2015.053

881 32. Laskowski RA, MacArthur MW, Moss DS, Thornton JM. PROCHECK: a program to
882 check the stereochemical quality of protein structures. J Appl Crystallogr. 1993;26(2):283–91.

883 33. Kaplan W, Littlejohn TG. Swiss-PDB Viewer (DeepView): An open-source molecular
884 modeling program. Brief Bioinform. 2001;2(2):195–7.

885 34. Milne GWA. Computer software review of ChemBioDraw 12.0. J Chem Inf Model.
886 2010;50(11):2053.

887 35. Morris GM, Lim-Wilby M. Molecular docking. Methods Mol Biol. 2008;443:365–82.

888 36. Racine J. The Cygwin tools: a GNU toolkit for Windows. J Appl Econom [Internet].
889 2000;15(3):331–41.

890 37. Salentin S, Schreiber S, Haupt VJ, Adasme MF, Schroeder M. PLIP: fully automated
891 protein–ligand interaction profiler. Nucleic Acids Res [Internet]. 2015;43(W1):W443–7.

892 38. Laskowski RA, Swindells MB. LigPlot+: multiple ligand-protein interaction diagrams for
893 drug discovery. J Chem Inf Model. 2011;51(10):2778–86.

894 39. Miyata T. Discovery Studio modeling environment. Ensemble. 2015;17:98–104.

895 40. DeLano WL. PyMOL: An open-source molecular graphics tool. CCP4 Newsl Protein
896 Crystallogr [Internet]. 2002;40:82–92.

897 41. Vallur AC, Tutterrow YL, Mohamath R, Pattabhi S, Hailu A, Abdoun AO, et al.
898 Development and comparative evaluation of two antigen detection tests for visceral
899 leishmaniasis. BMC Infect Dis. 2015;15:384.

900 42. Kapler GM, Coburn CM, Beverley SM. Stable transfection of the human parasite
901 Leishmania major delineates a 30-kilobase region sufficient for extrachromosomal replication
902 and expression. Mol Cell Biol. 1990;10(3):1084–94.

903 43. Pawar H, Puri M, Fischer-Weinberger R, Madhubala R, Zilberstein D. The arginine sensing
904 and transport binding sites are distinct in the human pathogen Leishmania. PLoS Negl Trop
905 Dis. 2019;13(1):e0007304.

906 44. Darlyuk I, Goldman A, Roberts SC, Ullman B, Rentsch D, Zilberstein D. Arginine
907 homeostasis and transport in the human pathogen Leishmania donovani. J Biol Chem.
908 2009;284(30):19800–7.

909 45. Fivelman QL, Adagu IS, Warhurst DC. Modified fixed-ratio isobologram method for
910 studying in vitro interactions between atovaquone and proguanil or dihydroartemisinin against
911 drug-resistant strains of Plasmodium falciparum. Antimicrob Agents Chemother.
912 2004;48(11):4097–102.

913 46. Akoachere M, Buchholz K, Fischer E, Burhenne J, Haefeli WE, Schirmer RH, et al. In vitro
914 assessment of methylene blue on chloroquine-sensitive and -resistant Plasmodium falciparum
915 strains reveals synergistic action with artemisinins. Antimicrob Agents Chemother.
916 2005;49(11):4592–7.

917 47. Kelly JX, Smilkstein MJ, Cooper RA, Lane KD, Johnson RA, Janowsky A, et al. Design,
918 synthesis, and evaluation of 10-N-substituted acridones as novel chemosensitizers in
919 Plasmodium falciparum. Antimicrob Agents Chemother. 2007;51(12):4133–40.

920 48. Hissin PJ, Hilf R. A fluorometric method for determination of oxidized and reduced
921 glutathione in tissues. Anal Biochem. 1976;74:214–26.

922 49. Rub A, Dey R, Jadhav M, Kamat R, Chakkaramakkil S, Majumdar S, et al. Cholesterol
923 depletion associated with Leishmania major infection alters macrophage CD40 signalosome
924 composition and effector function. Nat Immunol. 2009;10(3):273–80.

925 50. Lapara NJ 3rd, Kelly BL. Suppression of LPS-induced inflammatory responses in
926 macrophages infected with Leishmania. J Inflamm (Lond). 2010;7:8.

927 51. Kumari S, Kumar V, Tiwari RK, Ravidas V, Pandey K, Kumar A. Amphotericin B: a drug
928 of choice for visceral leishmaniasis. Acta Trop. 2022;235:106661.

929 52. Laniado-Laborín R, Cabrales-Vargas MN. Amphotericin B: side effects and toxicity. Rev
930 Iberoam Micol. 2009;26(4):223–7.

931 53. Wang X, et al. Sphingosine kinase 1: a potential therapeutic target for parasitic diseases. J
932 Parasitol Res. 2011;2011:1–10.

933 54. Cahill JL, et al. Sphingosine kinase 1 plays an essential role in the growth and viability of
934 Toxoplasma gondii. Int J Parasitol. 2009;39(9):1061–70.

935 55. Müller MA, et al. Synergistic effects of drug combinations for the treatment of Leishmania
936 infection. Antimicrob Agents Chemother. 2018;62(11):e01455-18.

937 56. Siqueira-Neto JL, et al. Sphingosine kinase inhibitors as promising new anti-leishmanial
938 agents: synergy with other drugs. J Antimicrob Chemother. 2014;69(3):667–74.

939 57. Gordon JR, et al. Characterization of sphingosine kinase 1 from Leishmania donovani and
940 its potential as a drug target. Mol Biochem Parasitol. 2012;183(1):1–9.

941 58. Pitson SM, et al. PF-543, a potent sphingosine kinase 1 inhibitor, reduces sphingosine-1-
942 phosphate production and blocks the growth of T-cell acute lymphoblastic leukemia cells. Mol
943 Cancer Ther. 2008;7(6):1559–68.

944 59. Bresnick AR, et al. Subcellular localization of sphingosine kinase 1 in Leishmania spp. and
945 its association with the parasite's membrane-bound structures. J Cell Sci. 2009;122(20):3732–
946 42.

947 60. Dunn TM, et al. The subcellular localization of sphingosine kinase 1 in mammalian cells:
948 implications for its function in cell signaling. J Lipid Res. 2010;51(10):3061–71.

949 61. Barauskas J, et al. Design and synthesis of small-molecule inhibitors of sphingosine kinase
950 1: a computational approach. Bioorg Med Chem. 2014;22(24):6625–35.

951 62. Kharel Y, et al. Overexpression of sphingosine kinase 1 confers partial resistance to
952 targeted therapy in cancer cells. Mol Cancer Ther. 2016;15(12):3084–93.

953 63. Foster LJ, et al. Sphingosine kinase inhibition: potential for selective targeting of microbial
954 pathogens in humans. Trends Pharmacol Sci. 2007;28(3):178–85.

955 64. Hernández-Ruiz J, et al. Inhibition of sphingosine kinase 1 reduces Leishmania infection
956 in macrophages by targeting parasite survival pathways. Parasite Immunol. 2010;32(11):730–
957 8.

958 65. Liu Y, et al. Ceramide generation in Leishmania: a potential target for therapeutic
959 intervention. J Lipid Res. 2012;53(10):2104–14.

960 66. Maceyka M, et al. Sphingosine kinase 1 and 2 as regulators of sphingolipid metabolism
961 and biological function. J Lipid Res. 2012;53(8):1397–409.

962 67. Rennie DE, et al. Sphingosine kinase 1 inhibition modulates cytokine production in T-cell
963 immune responses. J Immunol. 2015;194(3):1261–70.

964 68. Saviola AJ, et al. Sphingosine kinase 1 inhibition alters immune responses and enhances
965 anti-parasitic immunity. PLoS Pathog. 2013;9(5):e1003351.

966 69. Olivier M, et al. The role of tumor necrosis factor-alpha and interleukin-12 in host
967 resistance to Leishmania. Infect Immun. 2002;70(5):2771–5.

968 70. Müller M, et al. Amphotericin B for the treatment of leishmaniasis: progress and
969 limitations. Clin Infect Dis. 2015;60(2):217–28.

970 71. Al-Rawi MA, et al. Synergistic effects of PF-543 with amphotericin B against Leishmania
971 donovani: targeting sphingolipid metabolism and membrane integrity. Antimicrob Agents
972 Chemother. 2019;63(5):e02211-18.

973 72. Soliman MM, et al. Combination therapy for leishmaniasis: enhanced therapeutic efficacy
974 in Leishmania donovani-infected mouse models. Antimicrob Agents Chemother.
975 2014;58(10):5955–62.

976

977 **Figures:**

978

979

980

981

982

983

984

985

986 **Graphical Abstract:**

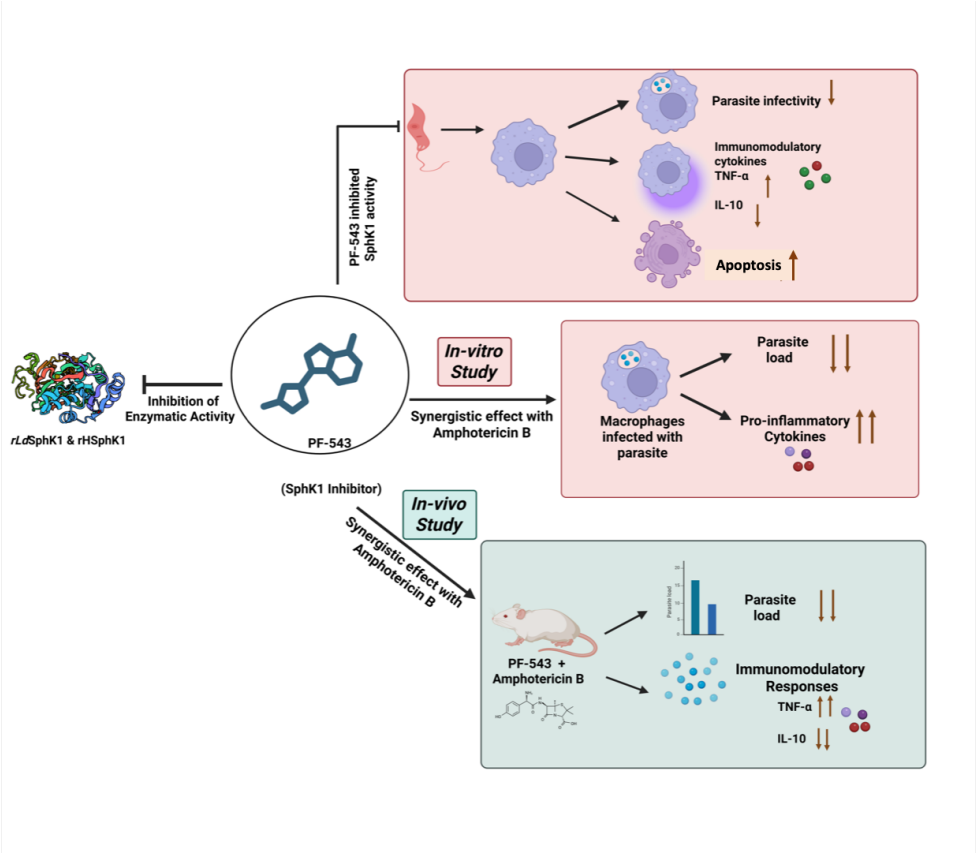

987

Fig 1

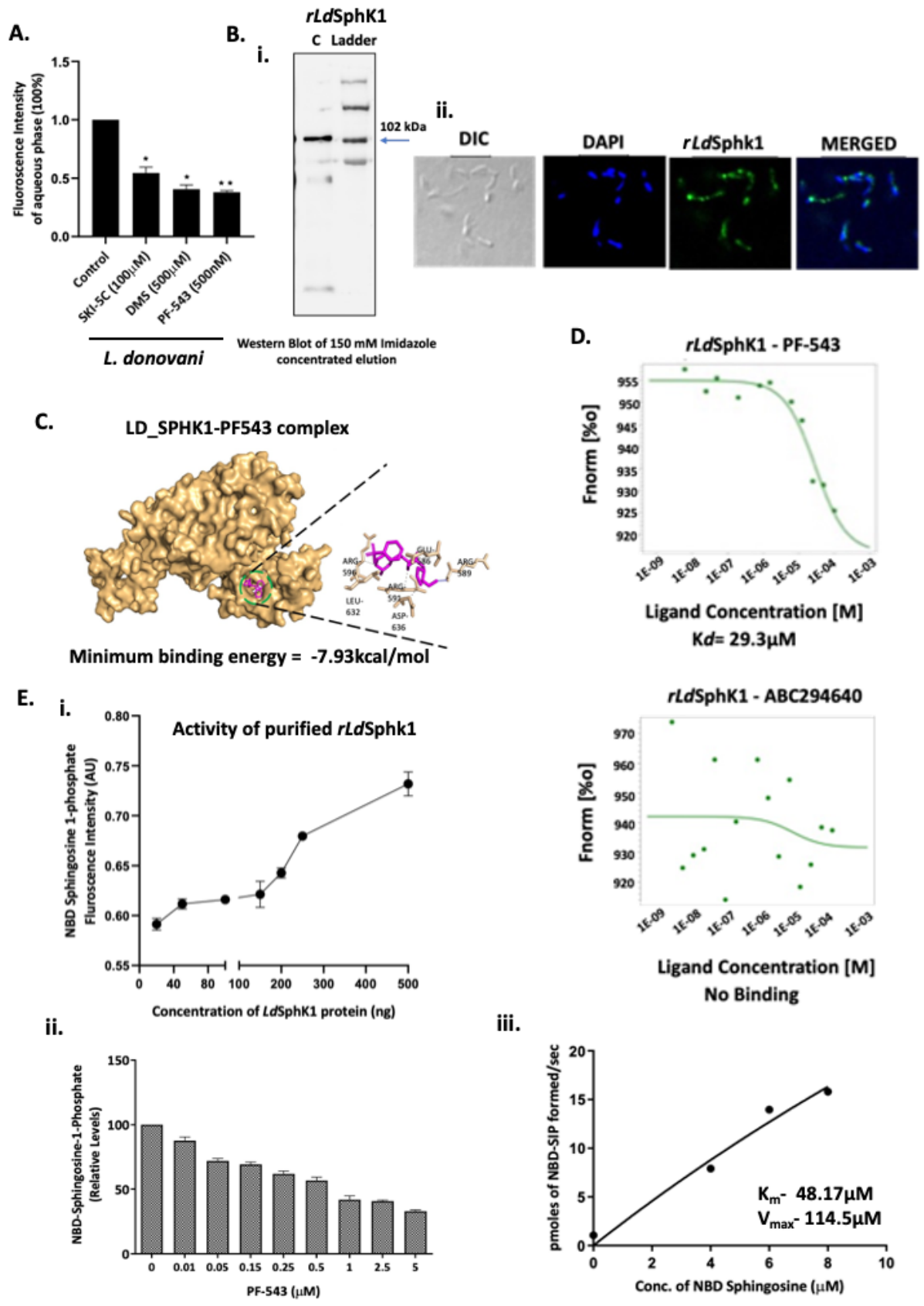
A.
Fluorescence Intensity of aqueous phase (100%)
1.5
1.0
0.5
0.0
Control
SKI-5C (100μM)
DMS (500μM)
PF-543 (500nM)
L. donovani
B.
i.
rLdSphK1
C Ladder
102 kDa
Western Blot of 150 mM Imidazole concentrated elution
ii.
DIC
DAPI
rLdSphk1
MERGED
C.
LD_SPHK1-PF543 complex
Minimum binding energy = -7.93kcal/mol
D.
rLdSphK1 - PF-543
Fnorm [%o]
955
950
945
940
935
930
925
920
1E-09
1E-08
1E-07
1E-06
1E-05
1E-04
1E-03
Ligand Concentration [M]
Kd= 29.3μM
E.
i.
Activity of purified rLdSphk1
NBD Sphingosine 1-phosphate Fluroscence Intensity (AU)
0.80
0.75
0.70
0.65
0.60
0.55
0
40
80
100
200
300
400
500
Concentration of LdSphK1 protein (ng)
rLdSphK1 - ABC294640
Fnorm [%o]
970
960
950
940
930
920
1E-09
1E-08
1E-07
1E-06
1E-05
1E-04
1E-03
Ligand Concentration [M]
No Binding
ii.
NBD-Sphingosine-1-Phosphate (Relative Levels)
150
100
50
0
0
0.01
0.05
0.15
0.25
0.5
1
2.5
5
PF-543 (μM)
iii.
pmoles of NBD-SIP formed/sec
20
15
10
5
0
0
2
4
6
8
10
Km- 48.17μM
Vmax- 114.5μM
Conc. of NBD Sphingosine (μM)

988

989

Fig 2

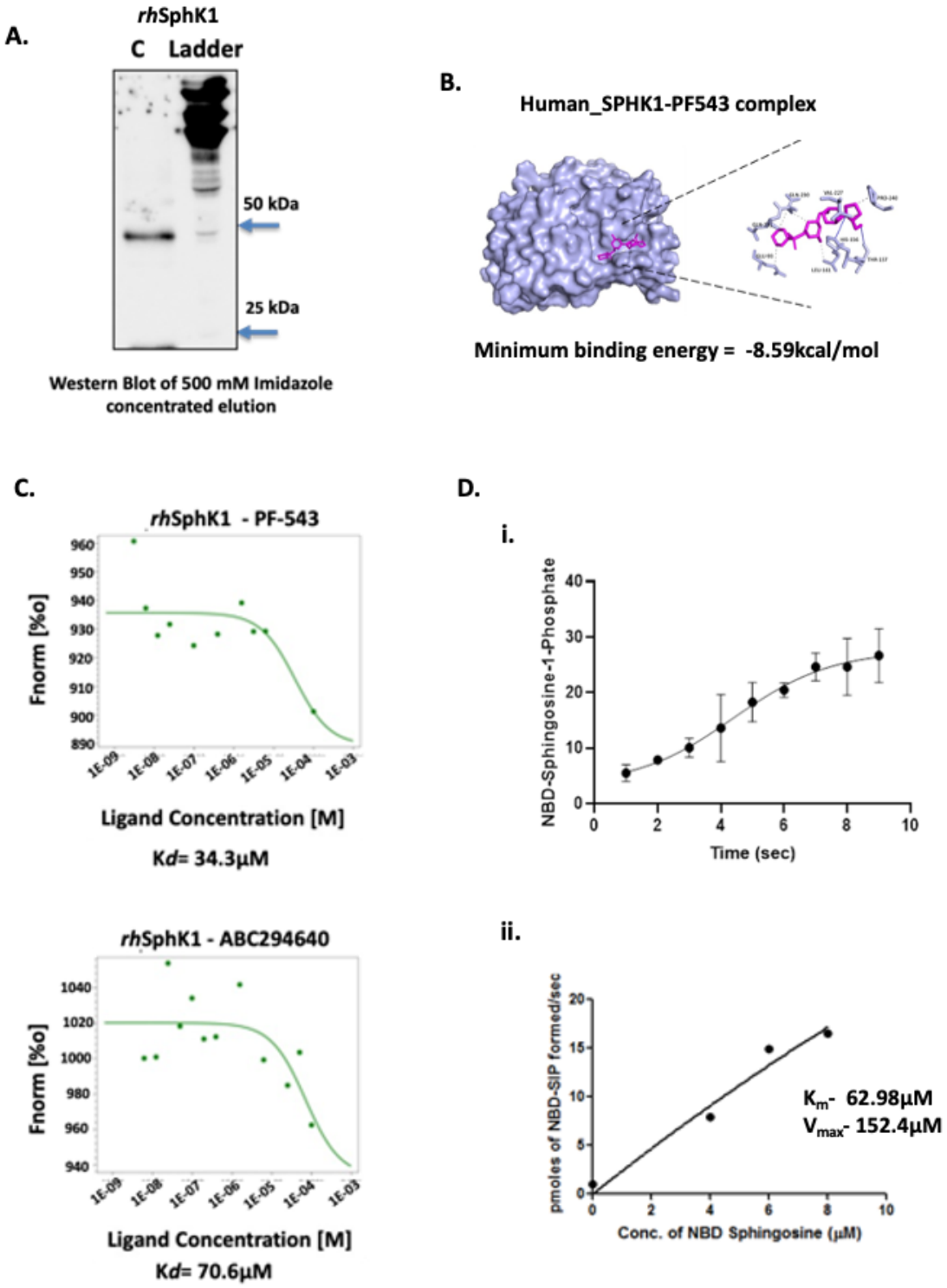
A.
rhSphK1
C Ladder
50 kDa
25 kDa
Western Blot of 500 mM Imidazole concentrated elution
B.
Human_SPHK1-PF543 complex
Minimum binding energy = -8.59kcal/mol
C.
rhSphK1 - PF-543
Fnorm [‰]
Ligand Concentration [M]
Kd= 34.3µM
rhSphK1 - ABC294640
Fnorm [‰]
Ligand Concentration [M]
Kd= 70.6µM
D.
i.
NBD-Sphingosine-1-Phosphate
Time (sec)
ii.
pmoles of NBD-SIP formed/sec
Conc. of NBD Sphingosine (µM)
Km- 62.98µM
Vmax- 152.4µM

990

991

Fig 3

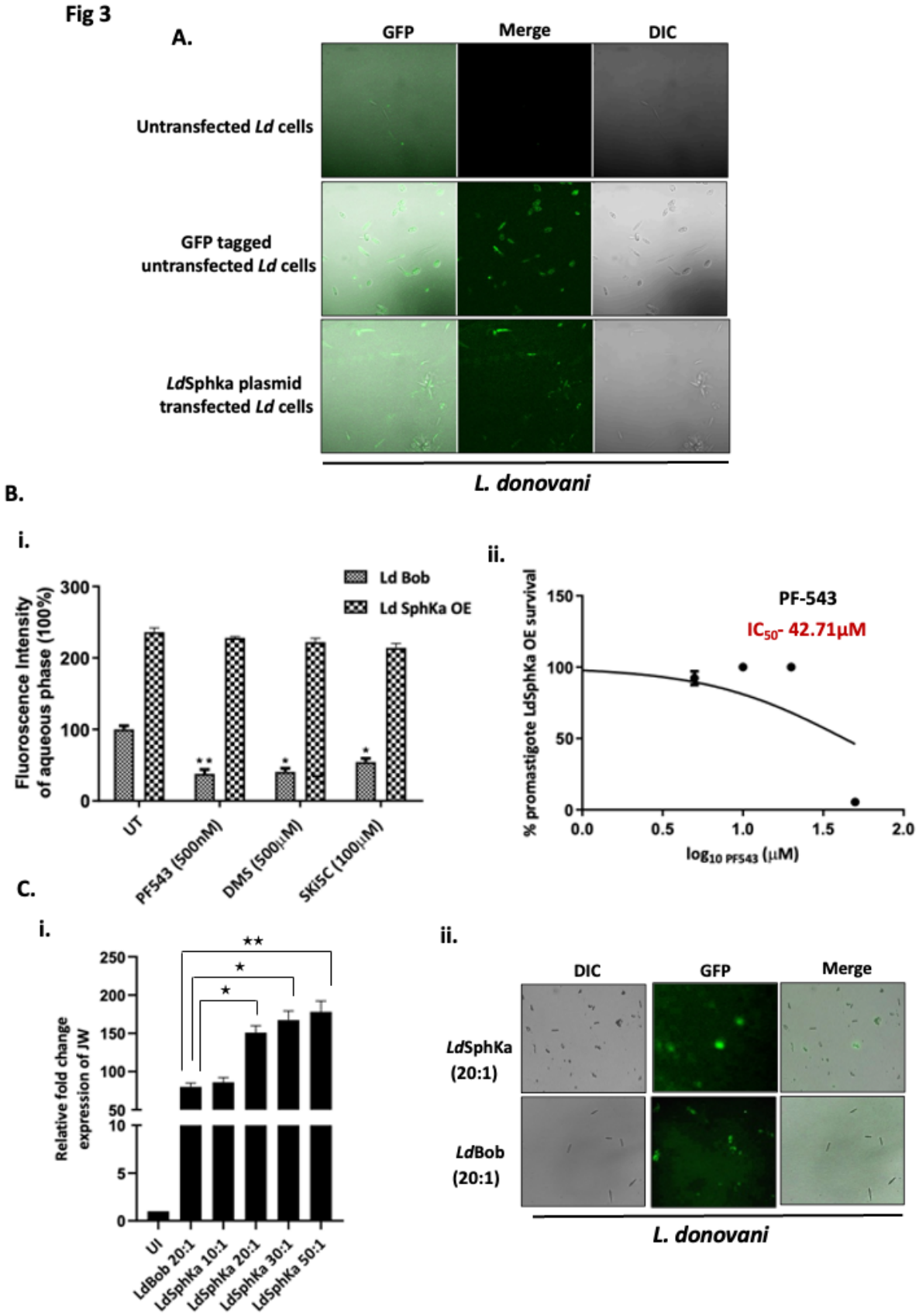
A.
GFP
Merge
DIC
Untransfected Ld cells
GFP tagged untransfected Ld cells
LdSphka plasmid transfected Ld cells
L. donovani
B.
i.
Ld Bob
Ld SphKa OE
Fluoroscence Intensity of aqueous phase (100%)
300
200
100
0
UT
PF543 (500nM)
DMS (500μM)
SKI5C (100μM)
ii.
PF-543
IC50- 42.71μM
% promastigote LdSphKa OE survival
150
100
50
0
0.0
0.5
1.0
1.5
2.0
log10 PF543 (μM)
C.
i.
Relative fold change expression of JW
250
200
150
100
50
10
5
0
UI
LdBob 20:1
LdSphKa 10:1
LdSphKa 20:1
LdSphKa 30:1
LdSphKa 50:1
ii.
DIC
GFP
Merge
LdSphKa (20:1)
LdBob (20:1)
L. donovani

992

993

Fig 4

A.

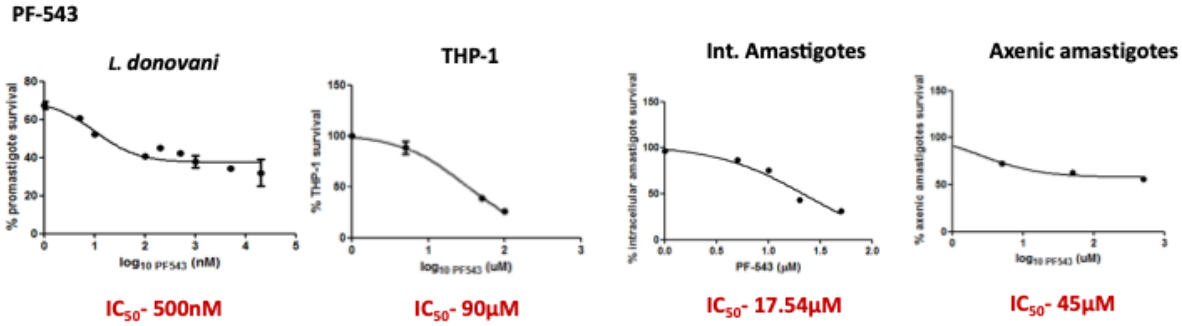

B.

i.

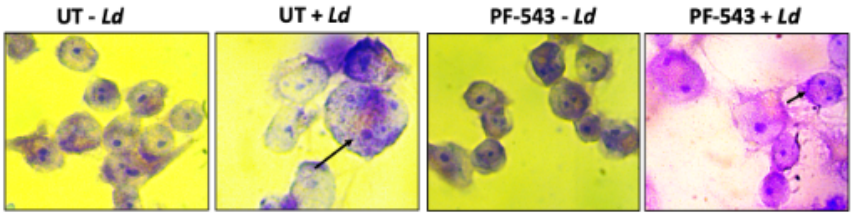

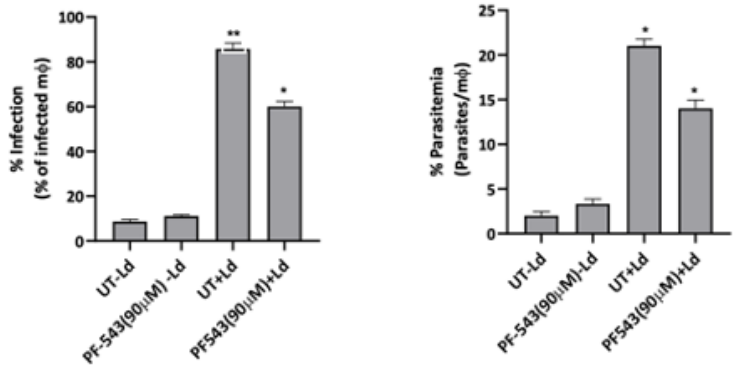

ii.

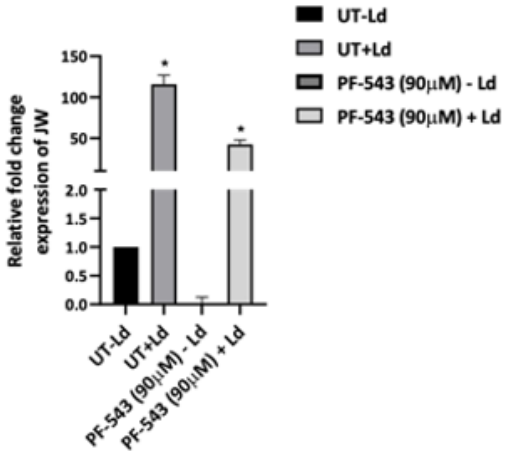

994

995

Fig 5

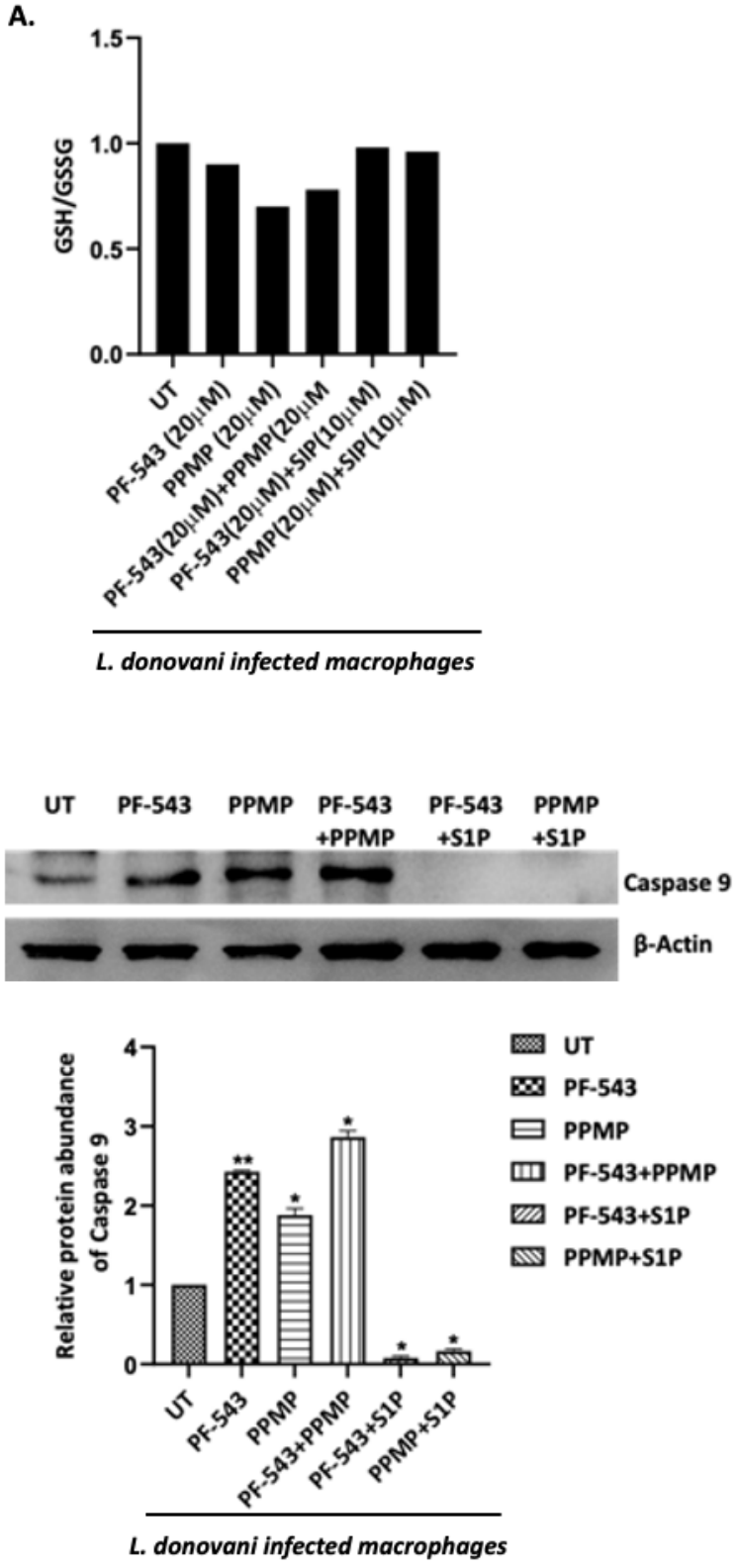
A.
GSH/GSSG
1.5
1.0
0.5
0.0
UT
PF-543 (20μM)
PPMP (20μM)
PF-543(20μM)+PPMP(20μM
PF-543(20μM)+SIP(10μM)
PPMP(20μM)+SIP(10μM)
L. donovani infected macrophages
B.
UT
PF-543
PPMP
PF-543 +PPMP
PF-543 +S1P
PPMP +S1P
Caspase 9
β-Actin
Relative protein abundance of Caspase 9
4
3
2
1
0
UT
PF-543
PPMP
PF-543+PPMP
PF-543+S1P
PPMP+S1P
L. donovani infected macrophages

996

997

Fig 6

A.

i.

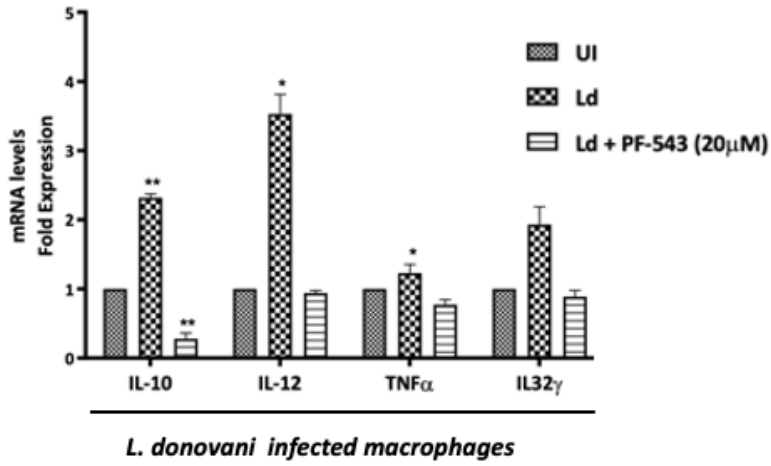

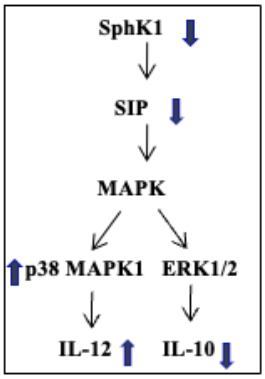

ii.

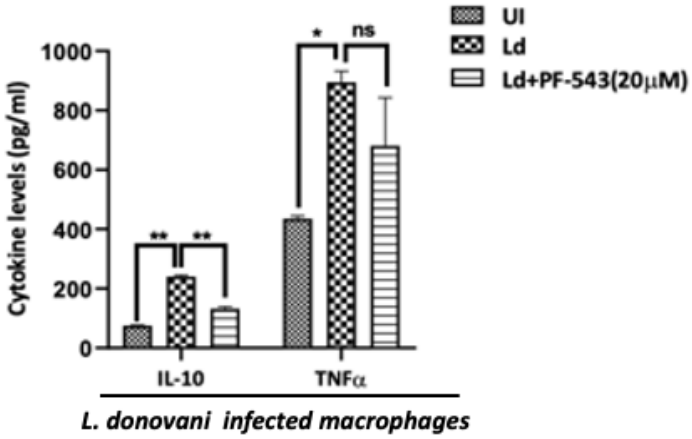

B.

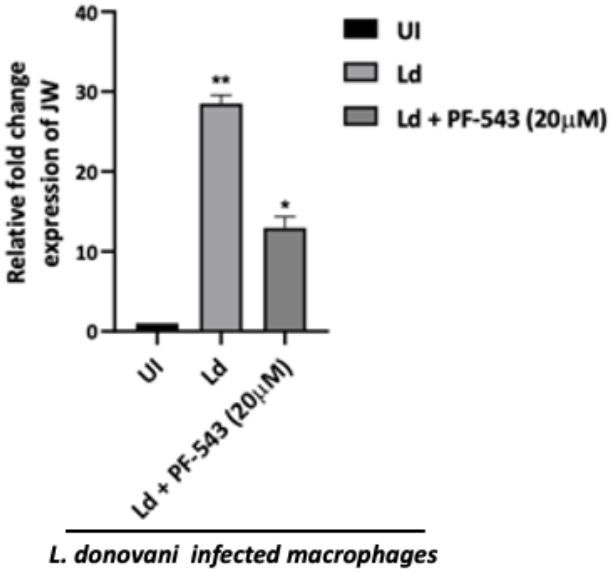

998

999

Fig 7

A.

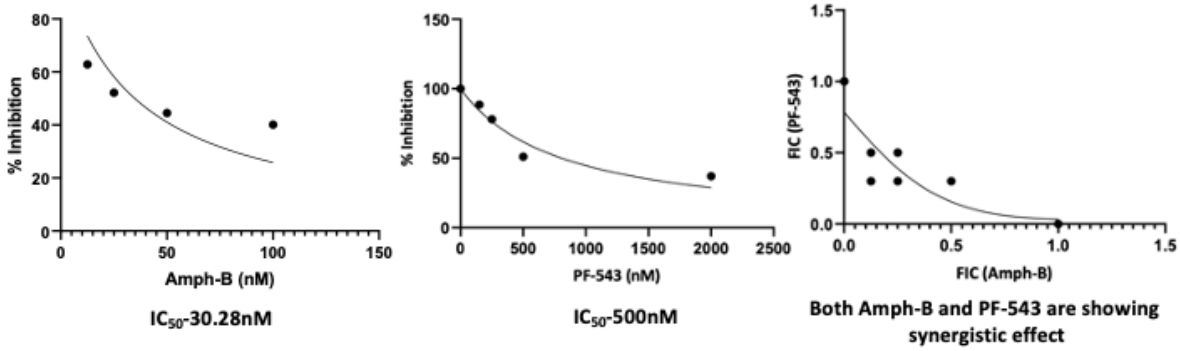

L. donovani

B.

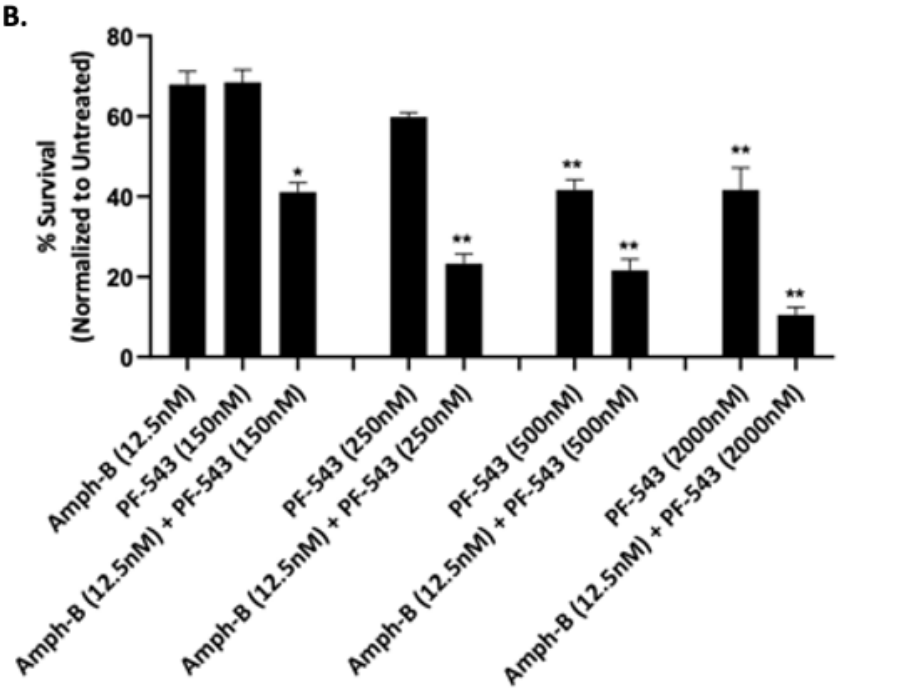

L. donovani infected macrophages

1000

1001

Fig 8

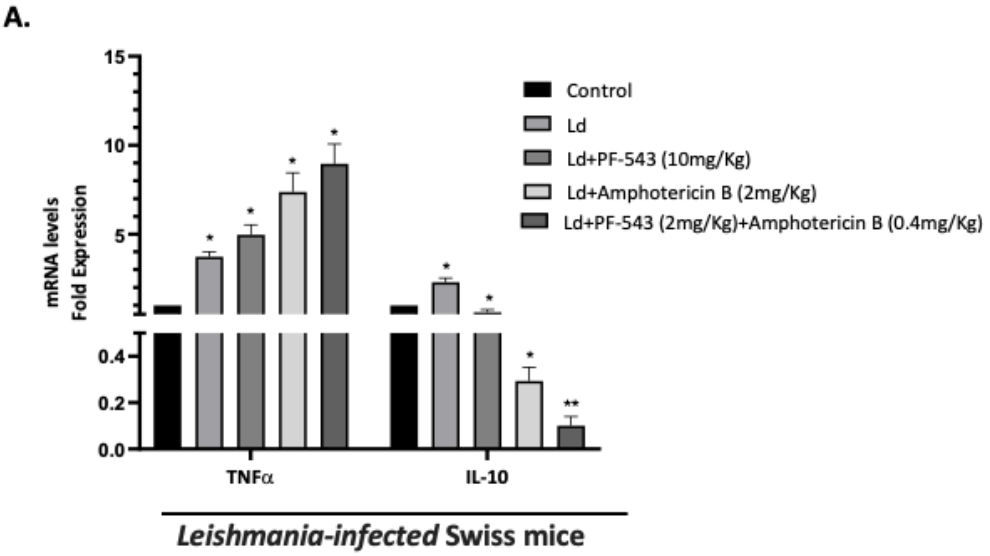

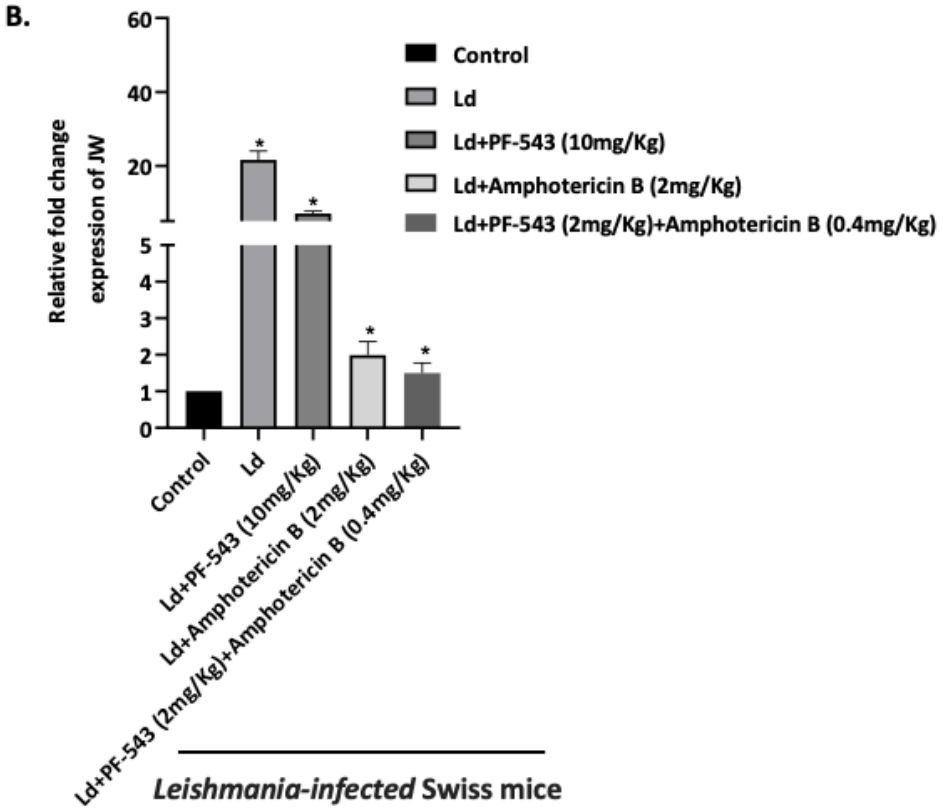

1002

1003

Fig S1

A. **LdBPK_260680.1.1**

2808 bp

```
ATGCACTCTTTCACCTCCAACAACACGCCGAGCCCTCAGTCGGCCACGCACCGCCACACGAACCACTCCGCTACAAACACCTCGTCGCTACTGCCGC
CGACCGCTTCACCGGTCCTGCAGGCGTCTTGTATGGATGCAAAGGAGGACCAAATTGACGCTGACGCGCAGGGTATTCCATCTTCAGTTCTCTCCAC
CTCAAAGGCGAGAATTTCCGCGGTGCCGACCAGCACCGAGTCCCCGCCATCGCGCGGCGCTGCTTACCAGCACGCCCCCGCCGGCAGCATCAATGAG
AGCGCAGCAACCGGCGCCACCGCAGTGCAGCACAGCGATTCAGGTAGCAGCACCGCAGCACCCACCGCGTCATCGTCGTCGCCACCGCCTCAGAAAC
AGCAGTCGCAACATCTCAAACCCGCTGCCTACCCTGGGAAGCTCGACGACGCTCCTCACGCCGTGAACGACAACATGGAAGCTGTCATCATCAACAA
GGGCAGGATCTGCACCCTTGCCTACTTCCCTAGTAGTGGCAACTTCCGCATCACGCACGTGTCAAGCACCGGCAAGACGCGCGTAGTCCTGAACATT
CCGGTGCGGACGATCATCAACATAGAGACCGCGGCTGAGCGTGACGCGCGGCAGCGAGCGCGCCAAGCGAACGACGACACAGTCAAACTTGCCTTTG
CCGAGAACGGGCGTAACACGGGAGGTCTTCTCTGCACCTTCCCCTCCGGCGCCGACGAGGACAACGAGACAGTGGTGTTTGCCCACTCCCGCGTCAA
CACAGCCTCCTTCACGCTGAGGTTGCTGGGCGGGCCCTCTCCCACACCGACTGCGTCGCACTTCGGCACGCACACAGCCGCTTGCGCGGTGACCACG
GCGGTGCCGAGCATCCGCTACTATGCCCACTACGTGCAGCAGCGCAACAAGGAGAACCCGTCTATCCGCACGCTAGAGTTCCAGTCGAGCGGCCCGG
CCGAGACGGTTCAGCATGTTGTGTCAACGGTGGTGCAGCGCATCTATCAGAAGGGCTCGAAGCACATCATCGCCTTTATTAGCGCCAAGTCAGGCAA
GGGAAAGGGTGAGCACATCTTCGAGAAGCAGGTGCGCCCCGTGCTGCACTTCAGCCGCCACACATACCAGGCTCACGTGACGCGCCGCGCGCATGAC
TGCGAGGACTACGTAGCAAACCTTGAGAACCCGATGAACAGCAACACCGTCATTGCCGCCGTTGGCGGAGACGGCATGATTCACGAAACTGTGAACG
GCGTGCACCGCCGCAAGCTGGCACTCGTGCGCTGGCTGCGCAGCGTGACAGCCGAGGGGAGCACCGGGGGCACGTCTGCCGTCTCGCCCAACGTGTC
TGCCCATCTGAACGAGGAGACGTGCGCGGCGGTGACACTAAAGTCGGGCGGCGCTAACAAAGTGGCGCCCCACGGCGAGGCCAGCGTCGGCTCTCCG
TCACCCTTCATTCAGCTGGGTTGTGAGGAGAACAAGCGTAACGGTTACGGCGGAAACGGTGCGACGCCTTCGGCGGAGGCGACGGCCCGAGAGGCTT
ATCGGCTTGCCCGCTGTCTGGTGCAAGACGGCTGGGATGCGCTGATGCCGCTCGTTGCGACGGTGGCGACCGGAAGCGCCTGCGGCCTTGCCAAGAG
CCTTGATGTCCTCTCCGTCGCCGAGGCAGCGTTGTCGCTGGTACACCTGAGCACGGTGCACATGGACCTGCTGTTGATGAACTTCACCCCGAACGAG
GATATGGTGGAGTTCCACCGCTGCCGTATGAGTGCGAGTCGACTCGACGCCGCACAGCGCGAGTTCTCGCAGTACAAGGAAGACAAGGCGGCCGAGC
TGCAGGAGCGATTGCGGCTGAGAGAGGCGCTCCAGCTGCCTCCCCGAATGCTGACGGCAGCCGACTGTATGACACCTTTCCTGAAGGATGGCTCGAA
CGTCTACCGCGACGCCGTCAGCTGCGCGACGCGGATGCCGGAGTTACACAGCCGTGTCGCCTTTATGTCGCTGTCGTTTGGCGCCGCGAACGACATC
GACCACGGCTCGGAGTCGTTGCGTTGGATGGGCAATGCCCGCTTCCACGTGTATGGTGGGTACATGATACTGCGTGGCCTCAAGCGGTACAAAGGCA
TGCTGCGTTACCTGCCGTGGGAGAGCAAGGCTGGCAAGACGGTGGAGAAGCTGCACACACGCTGCAAGATTCCATCGACAGATGACTTTCCGCTCTG
CACGATGCGGGAGAGCTGCCCGCACTGCCGCCAGTATGTGTTTGCCCACTGCGGCGCGCCGTCGCTCTCCTCGATGCAAGGCAATGACACGCATCCG
GGCCCAACTCCAAACACCAGCCGAGGCGCTGCCCAGCCCATTAGTGCCGCCGAAGCTCTAGCCCCATACACGGACCAGCAGTTGCTCGACGAGGACG
CTGTGGACTTCAAGGATGAGCGGCTCCCGTGGGTAACCATTCGCGGTGATTTCTGCATCGCACTCCTGTGCAACGTGCGGGATGTTGCGCAGGACAT
GCTCATGGCGCCGTTAGCACACATGTCGGATGGCGCCATCGATGTAGTCTACTGCCGCGTCGACCCCACCACGGGCCGCGGGAGGACGGATGGAGATG
CTGAAGTTCTTTATGGGTCTGGAGTCGGGTGCACACGTCAACCTCGACTTTGTGAACTACGTAAAGGCGCGCGCCTTGGAGATCAAGGTGGACGCCG
GCATCTCGATGTCGGACGGCGAGTTGATGCCGCTCAGCTCCGTGCGCGTGACGAAGATGCGCGGCAGCGTGCAGCTCGTGCGCAGTGGGTAG
```

Sphk1_BamHI_FP: GATGGGATCCATGCACTCTTTCACCTCCAA

Sphk1_XhoI_RP: ATTCTCGAGCTACCCACTGCGCACGAGCT

B.

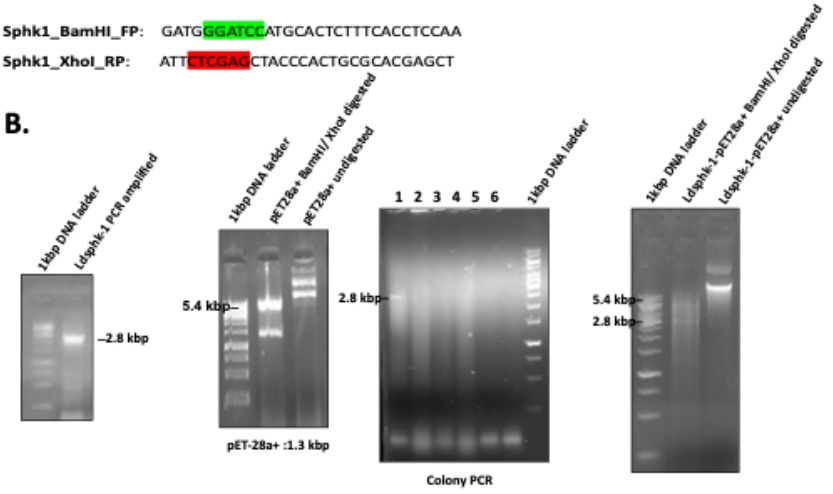

C.

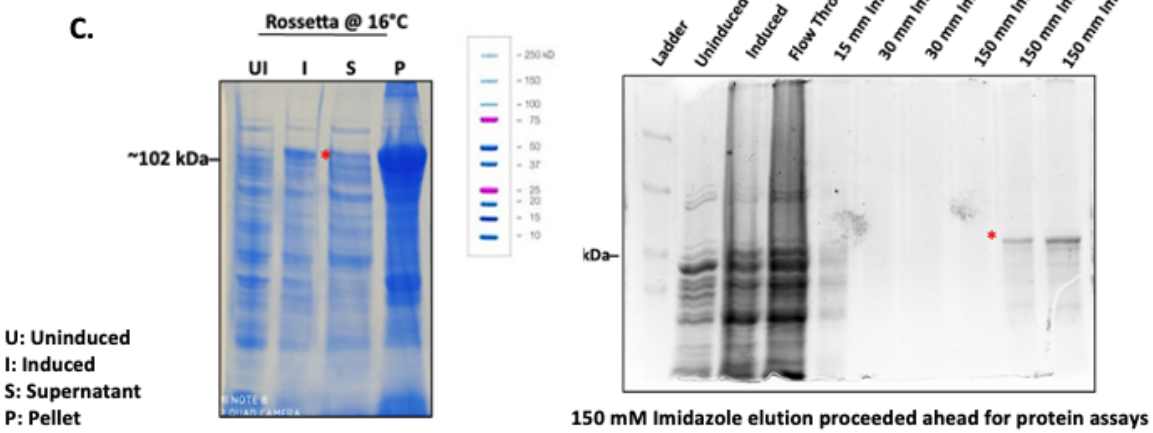

U: Uninduced
I: Induced
S: Supernatant
P: Pellet

150 mM Imidazole elution proceeded ahead for protein assays

Ldsphk-pET28a+ (Rossetta) at 16°C, 1mM IPTG induction was proceeded for protein purification

Fig S2

A.

E9BI81_LEIDO, Length: 935, Mass (Da):100,846

MHSFTSNNTPSPQSATHRHTNHSATNTSSLLPPTASPVLQASCMDAKEDQIDADAQGIP
SSVLSTSKARISAVPTSTESPPSRGAAYQHAPAGSINESAATGATAVQHSDSGSSTAAP
TASSSSPPPQKQQSQHLKPAAYPGKLDDAPHAVNDNMEAVIINKGRICTLAYFPSSGNF
RITHVSSTGKTRVVLNIPVRTIINIETAAERDARQRARQANDDTVKLAFAENGRNTGGL
LCTFPSGADEDNETVVFAHSRVNTASFTLRLLGGPSPTPTASHFGTHTAACAVTTAVPS
IRYYAHYVQQRNKENPSIRTLEFQSSGPAETVQHVVSTVVQRIYQKGSKHIIAFISAKS
GKGKGEHIFEKQVRPVLHFSRHTYQAHVTRRAHDCEDYVANLENPMNSNTVIAAVGGDG
MIHETVNGVHRRKLALVRWLRSVTAEGSTGGTSAVSPNVSAHLNEETCAAVTLKSGGAN
KVAPHGEASVGSPSPFIQLGCEENKRNGYGGNGATPSAEATAREAYRLARCLVQDGWDA
LMPLVATVATGSACGLAKSLDVLSVAEAALSLVHLSTVHMDLLLMNFTPNEDMVEFHRC
RMSASRLDAAQREFSQYKEDKAAELQERLRLREALQLPPRMLTAADCMTPFLKDGSNVY
RDAVSCATRMPELHSRVAFMSLSFGAANDIDHGSESLRWMGNARFHVYGGYMILRGLKR
YKGMLRYLPWESKAGKTVEKLHTRCKIPSTDDFPLCTMRESCPHCRQYVFAHCGAPSLS
SMQGNDTHPGPTPNTSRGAAQPISAAEALAPYTDQQLLDEDAVDFKDERLPWVTIRGDF
CIALLCNVRDVAQDMLMAPLAHMSDGAIDVVYCRVDPTTGRGGRMEMLKFFMGLESGAH
VNLDFVNYVKARALEIKVDAGISMSDGELMPLSSVRVTKMRGSVQLVRSG

B.

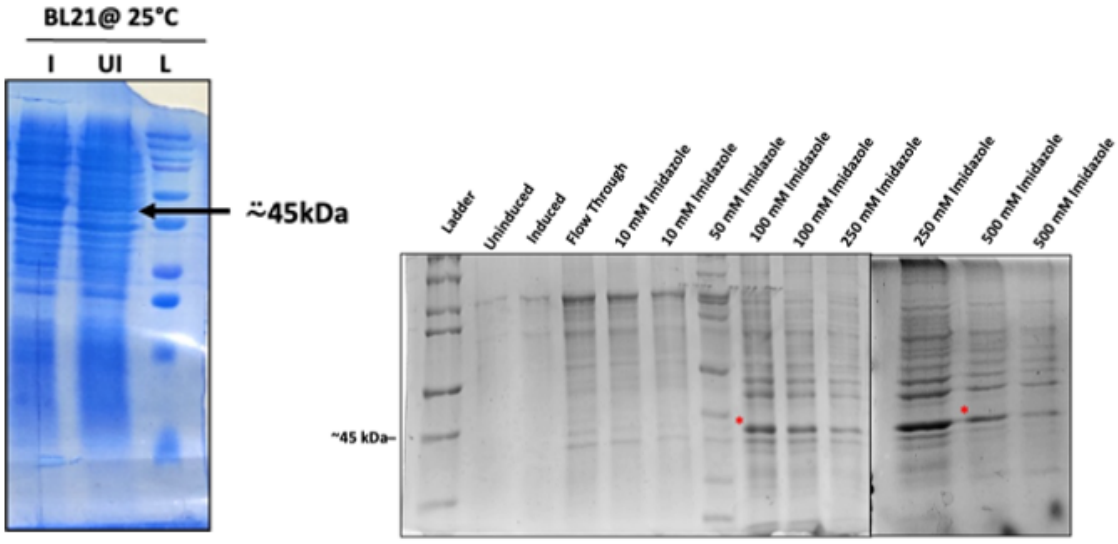

500 mM Imidazole elution proceeded ahead for protein assays

U: Uninduced
I: Induced
L: Ladder
pET-28 a(+) expression vector, and the recombinant plasmid was transformed into *E. coli* strain BL21 (λDE3) gold, 1mM IPTG induction was proceeded for protein purification

1006

1007

Fig S3

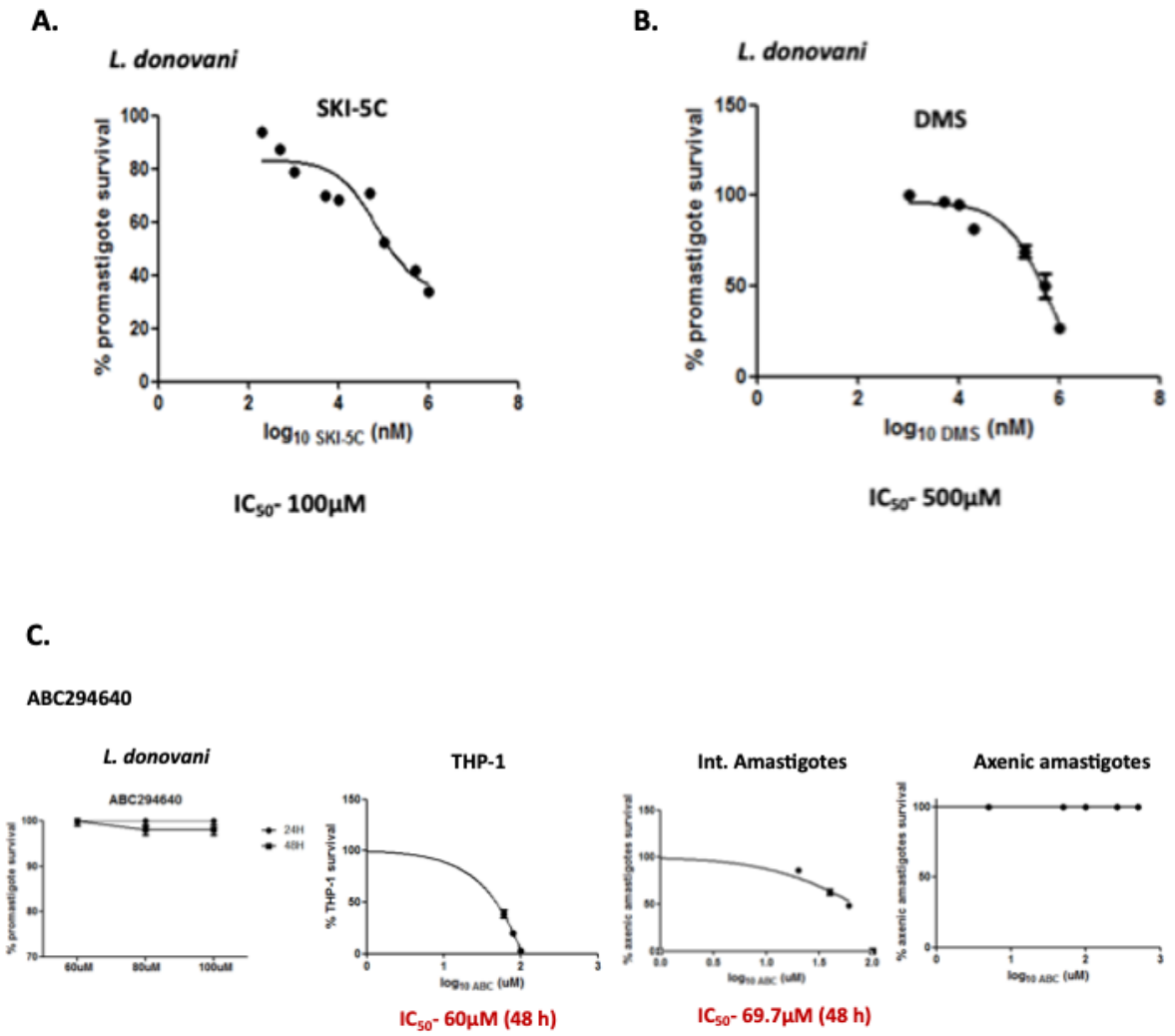

1008

1009

Fig S4

A.

```
CLUSTAL O(1.2.4) multiple sequence alignment

MHSFTSNNTPSPQSATHRHTNHSATNTSSLLPPTASPVLQASCMDAKEDQIDADAQGIPSSVLSTSKARISAVPTSTESP    PSRGAAYQHAPAGSINESAATGATAVQHSDSGSSTAAPTASSSSPPPQKQQSQHLKPAAY
MDPAGGPRGV                                                                          ------------------------------------------------------------

MHSFTSNNTPSPQSATHRHTNHSATNTSSLLPPTASPVLQASCMDAKEDQIDADAQGIPSSVLSTSKARISAVPTSTESP    PGKLDDAPHAVNDNMEAVIINKGRICTLAYFPSSGNFRITHVSSTGKTRVVLNIPVRTII
MDPAGGPRGV                                                                          ------------------------------------------------------------

MHSFTSNNTPSPQSATHRHTNHSATNTSSLLPPTASPVLQASCMDAKEDQIDADAQGIPSSVLSTSKARISAVPTSTESP    NIETAAERDARQRARQANDDTVKLAFAENGRNTGGLLCTFPSGADEDNETVVFAHSRVNT
MDPAGGPRGV                                                                          ------------------------------------------------------------

MHSFTSNNTPSPQSATHRHTNHSATNTSSLLPPTASPVLQASCMDAKEDQIDADAQGIPSSVLSTSKARISAVPTSTESP    ASFTLRLLGGPSPTPTASHTGTHTAACAVTTAVPSIRYYAHYVQQRNKENPSIRTLEFQS
MDPAGGPRGV                                                                          ------------------------------------------------------------

MHSFTSNNTPSPQSATHRHTNHSATNTSSLLPPTASPVLQASCMDAKEDQIDADAQGIPSSVLSTSKARISAVPTSTESP    SGPAETVQHVVSTVVQRIYQKGSKHIIAFISAKSGKGKGKHIFEKQVRPVLHFSRHTYQA
MDPAGGPRGV                                                                          ------------------------------------------------------------

MHSFTSNNTPSPQSATHRHTNHSATNTSSLLPPTASPVLQASCMDAKEDQIDADAQGIPSSVLSTSKARISAVPTSTESP    HVTRRAHDCEDYVANLENPMNSNTVIAAVGGDGMIHETVNGVHRRKLALVRNLRSVTAEG
MDPAGGPRGV                                                                          ------------------------------------------------------------

MHSFTSNNTPSPQSATHRHTNHSATNTSSLLPPTASPVLQASCMDAKEDQIDADAQGIPSSVLSTSKARISAVPTSTESP    STGGTSAVSPNVSAHLNEETCAAVTLKSGGANKVAPHGEASVGSPSPFIQLGCEENKRNG
MDPAGGPRGV                                                                          ------------------------------------------------------------

MHSFTSNNTPSPQSATHRHTNHSATNTSSLLPPTASPVLQASCMDAKEDQIDADAQGIPSSVLSTSKARISAVPTSTESP    YGGNGATPSAEATAREAYRLARCLVQDGWDALMPLVATVATG-SACGLAKSLDVLSVAEA
MDPAGGPRGV                                                                          ==================KELVRSEELGRWDALVVMSGDGLMHEVVNGL============
                                                                                                    .*.*.   . ****: : .        . **

MHSFTSNNTPSPQSATHRHTNHSATNTSSLLPPTASPVLQASCMDAKEDQIDADAQGIPSSVLSTSKARISAVPTSTESP    ALSLVHLSTVHMDLLLMNFTPNEDNVEFHRCRMSASRLD---AAQREFSQYKEDKAAELQ
MDPAGGPRGV                                                                          ----------------MERPDWETAIQKPLCSLPAGSGNALAASLNHYAGYEQVTNEDLL
                                                                                                  *:     *  ::   * : *.  :    *: ..:: *:: .  :*

MHSFTSNNTPSPQSATHRHTNHSATNTSSLLPPTASPVLQASCMDAKEDQIDADAQGIPSSVLSTSKARISAVPTSTESP    ERLRLREALQLPPRMLTAADCMTPFLKDGSNVYRDAVSCATRMPELHSRVAFMSLSFGAA
MDPAGGPRGV                                                                          TN----CTLLLCRRLLSPMNLLSLHTA-----------------SGLRLFSVLSLAWGFI
                                                                                     .     :* *  *:*:  : :: .                    .    .:.:**::*

MHSFTSNNTPSPQSATHRHTNHSATNTSSLLPPTASPVLQASCMDAKEDQIDADAQGIPSSVLSTSKARISAVPTSTESP    NDIDHGSESLHWMGNARFHVYGGYMILRGLKRYKGMLRYLPWESKAGKTVEKLHTRCKIP
MDPAGGPRGV                                                                          ADVDLKSEKYRRLGEMRFT-LGTFLRLAALRTYRGRLAYLPVGRVGSKTPASPVVVQ---
                                                                                     *:*  **. * :*: **   * :: * .*: *:* * ***    ..**  .  .

MHSFTSNNTPSPQSATHRHTNHSATNTSSLLPPTASPVLQASCMDAKEDQIDADAQGIPSSVLSTSKARISAVPTSTESP    STDDFPLCTMRESCPHCRQYVFAHCGAPSLSSMQGNDTHPGPTPNTSRGAAQPISAAEAL
MDPAGGPRGV                                                                          ========================================QGPVDAHLVPLEEPV======
                                                                                                                        **.         :*:

MHSFTSNNTPSPQSATHRHTNHSATNTSSLLPPTASPVLQASCMDAKEDQIDADAQGIPSSVLSTSKARISAVPTSTESP    APYTDQQLLDEDAVDFKDERLPWVTI-RGDFCIALLCNVRDVAQDMLMAPLAHMSDGAID
MDPAGGPRGV                                                                          ==================PSHWTVVPDEDFVLVLALLHSHLGSEMFAAPMGRCANGVMH
                                                                                                        *..:   ** :.*     .:..:*: **:.: : *.:.

MHSFTSNNTPSPQSATHRHTNHSATNTSSLLPPTASPVLQASCMDAKEDQIDADAQGIPSSVLSTSKARISAVPTSTESP    VVYCRVDPTTGRGGRMEMLKFFMGLESGAHVNLDF--VNYVKARAL--EIKVDAGISMSD
MDPAGGPRGV                                                                          LFYVRAGV-----SRAMLLRLFLAMEKGRHMEYBCPYLVYVPVVAFRLEPKDGKGVFAVD
                                                                                    :.* *..      .*  :*::*:.:*.* *:: :   : ** . *:  * * . *:   *

MHSFTSNNTPSPQSATHRHTNHSATNTSSLLPPTASPVLQASCMDAKEDQIDADAQGIPSSVLSTSKARISAVPTSTESP    GELMPLSSVRVTKMRGSVQLVRSG--------------------
MDPAGGPRGV                                                                          GELMVSEAVQGQVHPNY-FWMVSGCVEPPPSWKPQQMPPPEEPL
                                                                                    ****  .:*:     .    : **
```

B.

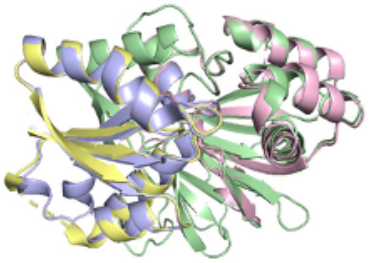

- Pink = LD_SPHK1
- Green = Human_SPHK1
- Blue = Human DAGKc domain
- Yellow = LD_ DAGKc domain

LD_ DAGKc doain get structurally aligned with human DAGKc domain

LD_SPHK1_DAGKc domain (DAG-kinase catalytic (DAGKc) = 341-425
Human_SPHK1_ DAGKc domain = 12-159

C.

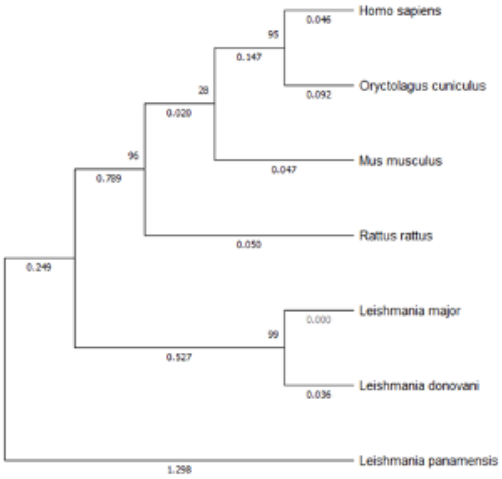

1010

1011

Fig S5

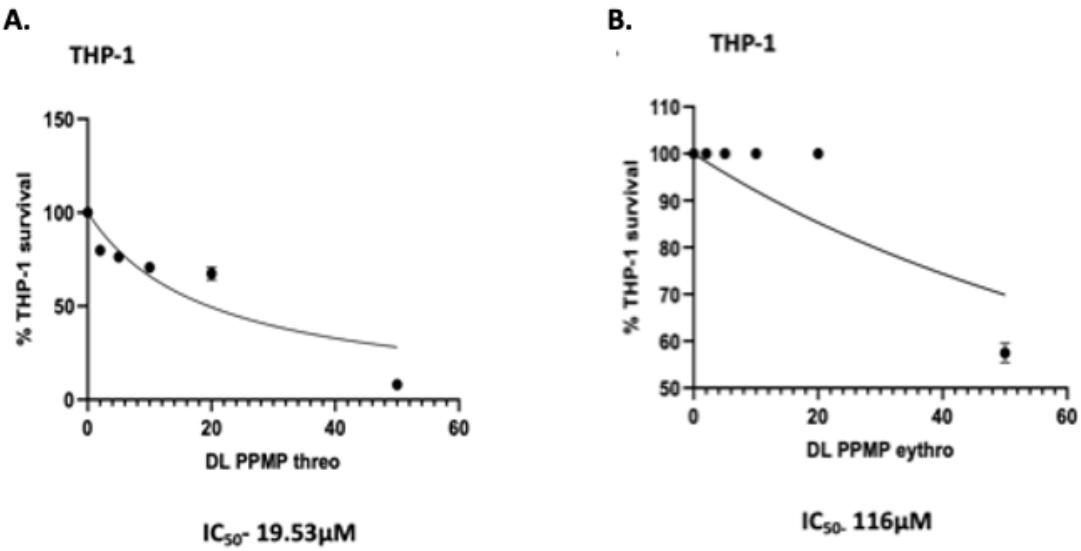

1012

1013

Table S1.

Primer	Sequence	Annealing Temperature
IL-10	Forward 5' –TTAAGGGTTACCTGGGTTGC-3' Reverse 5'-TGAGGGTCTTCAGGTTCTCC-3'	55°C
IL-12	Forward 5'-ATGCCCCTGGAGAAATGGTG-3' Reverse 5'-GGCCAGCATCTCCAAA CTCT-3'	55°C
IL-32γ	Forward 5'-AGGCCCGAATGGTAATGCT-3' Reverse 5'-CCACAGTG TCCTCAGTGTCACA-3	60°C
TNF-α	Forward 5'-CCTCTCTCTAATCAGCCCTCTG-3' Reverse 5'-GAGGACCTGGGAGTAGATGAG-3'	60°C
RNU6AP	Forward 5'-GGCCCAGCA GTACCTGTTTA-3' Reverse 5'-AGATGGCGGAGGTGCAG-3'	60°C
JW	Forward 5' CCTATTTTACACCAACCCCCAGT-3' Reverse 5'-GGGTAGGGGCGTTCTGCGAAA-3'	60°C
mIL-10	Forward 5'-AAATAAGAGCAAGGCAGTGG-3' Reverse 5'-GTCCAGCAGACTCAATACACAC-3'	60°C
mTNF-α	Forward 5'-TACTGAACTTCGGGGTGATTGGTCC-3' Reverse 5'-CAGCCTTGTCCCTTGAAGAGAACC-3'	60°C

1014

1015

1016 **Figure legends :**

1017 **Fig 1. (A) Estimation of *Ld*SphK-1-mediated generation of NBD-SIP levels against SphK**
1018 **inhibitors in *L. donovani* promastigotes.** *L. donovani* bob promastigotes were cultured in 25
1019 cm^2 flasks followed by treatment with SphK inhibitors; PF-543, DMS and SKI-5C for 48h.
1020 Inhibition of SphK1 using these SphK inhibitors cause decreased S1P levels. SphK inhibitor
1021 treated promastigotes were resuspended in buffer containing fatty acid-free BSA (0.1% (w/v))
1022 followed by resuspension in buffer containing BSA (1% (w/v)) and incubated with NBD-
1023 sphingosine (10µM) for 45 min at 37 °C. Promastigotes incorporate NBD-sphingosine (NBD-
1024 Sph), which are phosphorylated by Sphingosine kinase (SphK1) to NBD-S1P. Bar graph
1025 depicts ELISA-based S1P quantification in promastigotes treated with inhibitors. **(B)**
1026 **Purification and sub-cellular localization of Recombinant *rLd*SphK1 in *L. donovani*.**
1027 Concentrated r*Ld*SphK1 protein. (i) Gel image showing a purified band of 102kDa recombinant
1028 *Ld*SphK1 (ii) The subcellular localization of recombinant *Ld*SphK1 was investigated in
1029 promastigotes. Panel A: DIC at 60X. Panel B: DAPI. Panel C: anti-*Ld*SphK1 antibody detected
1030 using FITC (green)-conjugated secondary antibody. Panel D: merged micrographs. *Ld*SphK1
1031 expression represented in the green channel. Co-localization shown as the merged image. **(C)**
1032 ***In silico* docking of the *rLdSphK1* in presence of PF-543.** *In-silico* ligand-substrate
1033 interaction was done using Autodock 1.5.7rc1 and Cygwin terminal. The *in silico* docking
1034 generated the complex of *rLdSphK1*-PF-543 and represented as surface model highlighted with
1035 residues involved in the interaction using Chimera, Ligplus, Discovery Studio v19.1.0, and
1036 PyMOL v2.3.2 software. **(D) Biophysical interaction and functional characterization of the**
1037 ***rLdSphK1* (20µM) in presence of PF-543 (500nM, 1µM, 2.5µM, 5µM, 10µM, 20µM).** MST
1038 analysis confirms the interaction between *rLdSphK1* and PF-543. Dose-response curves of
1039 *rLdSphK1*–PF-543 showed K_D of 29.3µM. **(E) Analysis of functional characterization and**
1040 **catalytic activity of the *Ld*SphK1 recombinant protein.** (i) Time kinetics of activity of

1041 purified *rLd*SphK1 and NBD-S1P-based fluorometric assay showing increase in NBD-SIP
1042 levels in presence of different concentrations of *rLd*SphK1 protein. (ii) The inset shows
1043 inhibition of NBD-SIP levels in the presence of different concentrations of PF-543 using 200ng
1044 of recombinant *Ld*SphK1. (iii) Varying different concentration of NBD Sphingosine (2-10µM)
1045 and keeping *rLd*SphK1 constant (200ng), NBD-SIP levels were measured to calculate K_m and
1046 V_{max} of *rLd*SphK1. The plate was immediately placed on the varioskan LUX Multimode
1047 Microplate Reader (Thermo fisher, Massachusetts, USA) every 5 seconds for 20 min.
1048
1049 **Fig 2. (A) Purification of Recombinant *rhSphK1* from Supernatant.** Gel image showing a
1050 concentrated *rhSphK1* protein band of 50kDa. **(B) *In silico* docking of the *rHumanSphK1* in**
1051 **presence of PF-543.** *In silico* ligand-substrate interaction was done using Autodock 1.5.7rc1
1052 and Cygwin terminal. The *in silico* bound complex of *rhSphK1*-PF-543 was represented as
1053 surface model highlighted with residues involved in the interaction using Chimera, Ligplus,
1054 Discovery Studio v19.1.0, and PyMOL v2.3.2 software. The list of residues involved in
1055 hydrophobic interaction and hydrogen bond formation were highlighted in the model. **(C)**
1056 **Functional characterization of the *rhSphK1* in presence of PF-543.** MST analysis confirms
1057 the biophysical interaction between *rhSphK1* **-**PF-543 and *rhSphK1*-ABC294640, which was
1058 used as a control. Dose-response curves of PF-543 (20µM) and ABC294640 showed K_D of
1059 34.3µM and 70.6µM respectively. **(D) Analysis of catalytic activity of the *rhSphK1* using**
1060 **NBD-S1P-based fluorometric assay. (i)** Time kinetics of activity of purified *rhSphK1*
1061 demonstrated increase in NBD-SIP levels in presence of 200ng of *rhSphK1* protein. **(ii)**
1062 Varying different concentration of NBD Sphingosine (2-10µM) and keeping *rhSphK1* constant
1063 (200ng), NBD-SIP levels were measured to calculate K_m and V_{max} of *rhSphK1*. The readings
1064 were recorded every 5 seconds for 20 min using varioskan LUX Multimode Microplate Reader
1065 (Thermo fisher, Massachusetts, USA).

1066

1067 **Fig 3. Effect of PF-543 on cytotoxicity and infectivity of *L. donovani* SphK1 overexpressor**
1068 **promastigote cell line (A)** Detection of the presence of GFP encoded SphKa plasmid in
1069 *Leishmania donovani* parasites. *L. donovani* bob promastigotes were cultured in 25 cm^2 flasks
1070 followed by transfection with GFP-tagged SphKa plasmid. **(B (i)) Estimation of *Ld*SphK-1-**
1071 **mediated generation of NBD-SIP levels against PF-543 in *L. donovani* SphKa**
1072 **promastigotes.** *L. donovani* bob promastigotes were cultured in 25 cm^2 flasks followed by
1073 treatment with SphK1 inhibitor; PF-543 for 48h. Inhibition of SphK1 using PF-543 had no
1074 significant effect on S1P levels. SphK inhibitor treated SphKa promastigotes were resuspended
1075 in buffer containing fatty acid-free BSA (0.1% (w/v)) followed by resuspension in buffer
1076 containing BSA (1% (w/v)) and incubated with NBD-sphingosine (10μM) for 45 min at 37 °C.
1077 Promastigotes incorporate NBD-sphingosine (NBD-Sph), which are phosphorylated by
1078 Sphingosine kinase (SphK1) to NBD-S1P. Bar graph depicts ELISA-based S1P quantification
1079 in SphKa promastigotes treated with PF-543. **(ii) Effect of SphK1 inhibitor; PF-543 in**
1080 ***Leishmania* overexpressor *spp*.** To evaluate the IC_{50} for PF543, approximately 5×10^4 *Ld*
1081 *SphKa* Bob cells were seeded in each well of 96-well flat bottom plates and supplemented with
1082 M199 media containing PF-543 (200μl/well). The IC_{50} was found to be 42.71μM for
1083 *Leishmania donovani* SphKa promastigotes. Each experiment was done in triplicates and
1084 repeated thrice. **(C (i)) Effect of infectivity of *L. donovani* SphK1 overexpressor on the**
1085 **clearance of intracellular parasite load.** THP-1 macrophages were cultured in six-well plates
1086 in the presence or absence of *L. donovani* infection (MOI , 20:1) for 6h. Further, THP-1 cells
1087 were infected with *L. donovani* SphK1 overexpressor promastigotes at various MOIs (10:1,
1088 20:1, 30:1, 50:1). Infected THP-1 were washed to remove non-internalized parasites. Total
1089 RNA was enriched using TRIzol and the resulting cDNA was subjected to real-time PCR
1090 analysis using primers specific for infectivity (JW) genes in infected macrophages. RNU6A

1091 was used as a housekeeping gene. The results are expressed as fold-change of uninfected THP-
1092 1 cells. Statistical significance was quantified using the unpaired t-test. The data is a
1093 representation of mean ± SD from three independent experiments *, $p < 0.05$; ***, $p < 0.001$.
1094 **(C (ii)) Analysis of GFP expression in *L. donovani* SphK1 overexpressor and wild type**
1095 **promastigote cell lines.** Detection of the presence of GFP encoded SphKa and *Bob* plasmids
1096 in *Leishmania donovani* and *Leishmania* overexpressor parasites. *L. donovani bob* and *L.*
1097 *donovani* overexpressor promastigotes were cultured in 25 cm^2 flasks followed by confocal
1098 microscopy.
1099
1100 **Fig 4. (A) Effect of SphK1 inhibitors; PF-543 and ABC294640 in *Leishmania spp* and host**
1101 **macrophages.** To evaluate the IC_{50} for PF543, approximately 6×10^3 THP-1 and 5×10^4 *Ld* Bob
1102 cells were seeded in each well of 96-well flat bottom plates and supplemented with RPMI and
1103 M199 media containing PF-543 (200µl/well) respectively. For intracellular amastigotes, 1 ×
1104 10^6 THP-1 cells, treated with 50 ng/ml of phorbol 12-myristate 13-acetate (PMA) were seeded
1105 on glass coverslip in a 6-well plate for 48h. They were infected with late log-phase *L. donovani*
1106 promastigotes and simultaneously treated with PF-543. The cells were further incubated for 2
1107 days at 37°C and 5% CO_2. To determine, the intracellular parasite burdens (mean number of
1108 amastigotes per macrophage) were microscopically assessed using Giemsa staining. For axenic
1109 amastigotes, the axenically cultured forms grew optimally at a temperature of 32-33°C in a
1110 growth media with pH of 5.4. The IC_{50} were found to be 500nM, 90µM, 17.54µM and 45µM
1111 for *Leishmania donovani* promastigotes, THP-1 macrophages, intracellular amastigotes and
1112 axenic amastigotes respectively. Each experiment was done in triplicates and repeated thrice.
1113 **(B) Effect of Sphk1 inhibition on parasite infectivity in THP-1 macrophages.** THP-1 cells
1114 grown in RPMI medium were treated with SphK1 inhibitor; PF-543 for 24h followed by
1115 infection with *L. donovani* promastigotes at an MOI of 20:1 for 48h. (i) After 48h of infection,

1116 Giemsa staining was performed to assess the parasite burden. THP-1 cells were fixed, Giemsa
1117 stained and amastigotes were counted visually. Virulence capacity was determined by
1118 calculating infectivity (left panel) and parasitemia (right panel). Untreated infected THP-1 cells
1119 were used as control. (ii) Total RNA was enriched using TRIzol. Infectivity was validated using
1120 qRT-PCR with primer specific marker JW as a molecular indicator. Expression of JW mRNA
1121 in infected cells inferred parasite load and represented as percentage infectivity. Data analysis
1122 was performed using the $2^{-\Delta\Delta CT}$method. The results are representative of three independent
1123 experiments. Statistical significance was quantified using the unpaired t-test. The results
1124 signify mean ± S.D with n = 3, *P < 0.05.
1125
1126 **Fig 5. (A, B) Estimation of glutathione and Caspase 9 levels upon PF-543 treatment in**
1127 ***Leishmania* infected macrophages.** THP-1 macrophages were cultured in six-well plates in
1128 the presence of *L. donovani* infection (MOI, 20:1) for 6h. Infected THP-1 were washed to
1129 remove non-internalized parasites and treated with PF-543 (20μM) or DL-threo-PPMP;
1130 glucosylceramide synthase inhibitor (20μM) or SIP (10μM) for next 48h. GSH/GSSG and
1131 Caspase-9 levels were analysed using cell lysates quantified for GSG/GSSH assay and Western
1132 blot. Band intensities were quantified by ImageJ software and were plotted in GraphPad Prism.
1133 Data from one of three experiments is shown.
1134
1135 **Fig 6 (A(i), B) Effect of PF-543 on the expression of inflammatory molecules and**
1136 **clearance of intracellular parasite load.** THP-1 macrophages were cultured in six-well plates
1137 in the presence or absence of *L. donovani* infection (MOI, 20:1) for 6h. Infected THP-1 were
1138 washed to remove non-internalized parasites and treated with PF-543 for next 48h. Total RNA
1139 was enriched using TRIzol and the resulting cDNA was subjected to real-time PCR analysis
1140 using primers specific for inflammatory (IL32γ, IL-12 , IL-10 and TNF-α) and infectivity (JW)

1141 genes in PF-543 treated and untreated infected macrophages. RNU6A was used as a
1142 housekeeping gene. The results are expressed as fold-change of uninfected THP-1 cells.
1143 Statistical significance was quantified using the unpaired t-test. The data is a representation of
1144 mean ± SD from three independent experiments *, $p < 0.05$; ***, $p < 0.001$. **(A (ii))** Graph
1145 represents cytokine levels measured by sandwich ELISA. Statistical significance was
1146 quantified using the unpaired t-test with Welch's correction, in LPS-stimulated, *Ld*-infected
1147 and PF-543 treated macrophages.
1148
1149 **Fig 7. (A-B). Evaluation of PF-543 and Amphotericin B formulation on cytotoxicity or**
1150 **metabolic viability of *Leishmania* promastigotes and intracellular amastigotes. (A)** To
1151 determine the combinatorial impact of PF-543 and Amphotericin B formulation, promastigotes
1152 of *L. donovani* were seeded in 96-well plates (3×10^6 parasite/mL) in exponential growth phase
1153 at increasing concentrations (12.5nM–500nM) of Amphotericin B and (150nM- 2000nM) of
1154 PF-543 compounds and maintained at 26°C. After 48 h of incubation, the IC_{50} was determined
1155 by MTT assay. The absorbance was measured in a MultiskanEX photometric plate reader for
1156 microplates at 540 nm. Data were obtained from three independent experiments performed in
1157 triplicate. The fractional inhibitory concentration index (FIC) was evaluated to determine the
1158 synergistic activity of lead compounds; PF-543 with Amph-B. Finally, FIC < 0.5 represented
1159 strong synergistic activity between two drugs. While FIC > 4 is was considered as the
1160 antagonistic activity. FIC values were obtained from three independent experiments. **(B)** For
1161 validating the antileishmanial activity by PF-543 and Amphotericin B formulation on
1162 intracellular amastigotes, qPCR-based analysis was performed for all the treatments. For the
1163 same, THP-1 cells were seeded at a concentration of 8×10^5 cells/mL in 96-well plates and
1164 incubated for 24h with PMA (10ng/mL) supplemented with RPMI 1640. Following 24h
1165 priming with PMA, the culture medium was removed, and the cells were infected with *L.*

1166 *donovani* followed by treatment with the formulations having concentrations kept similar as
1167 used previously for promastigotes at 37°C and 5% CO_2. Total RNA was extracted, and the
1168 resulting cDNA was subjected to real-time PCR analysis using primers specific for kinetoplast
1169 minicircle DNA (kDNA)/JW of *L. donovani*. This primer does not match to human genome,
1170 thus directly indicates the intracellular parasite load against the treatments. Data analysis was
1171 performed using the $2^{-\Delta\Delta CT}$method.Values are mean ± S.D (n = 3). The results are representative
1172 of three independent experiments performed in triplicates.
1173
1174 **Fig 8. Expression of JW and inflammatory markers upon PF-543 treatment in**
1175 ***Leishmania-infected* Swiss mice.** Evaluation of the **(A)** immunomodulatory potential and **(B)**
1176 infectivity of PF-543 and Amph-B in *Leishmania*-infected Swiss mice was performed.
1177 10mg/Kg of PF-543 and 2mg/Kg of Amphotericin B alone were given for individual treatment
1178 in *Leishmania* infected mice. For constituting the synergistic effect of two drug partners;
1179 2mg/Kg (1mM) of PF-543 and 0.4mg/Kg (0.12μM) of Amphotericin B were prepared in
1180 1XPBS and given together to a mouse weighing 30gm. To evaluate the parasitemia and
1181 expression of inflammatory markers in infected mice upon drug administration, spleen was
1182 harvested from each group of mice and qRT-PCR analysis was performed using primers
1183 specific for inflammatory markers *IL-10 and TNFα* and parasite specific kinetoplast minicircle
1184 gene, *JW* in PF-543 and Amph-B treated infected mice in respect to the untreated Swiss mice.
1185 RNU6A (RNA, U6 small nuclear 1; THP-1 cells) was used as a housekeeping gene. The results
1186 were expressed as normalized fold-change of respective control. Statistical significance was
1187 quantified using the unpaired t-test. The data is a representation of mean ± SD from three
1188 independent experiments *, $p < 0.05$; ***, $p < 0.001$.
1189

1190 **Fig S1. (A) Nucleotide sequence encoding full length sequence of *L. donovani* Sphk1 (1-**
1191 **2808 bp).** This sequence was selected for recombinant protein generation as a fusion protein
1192 with an N-terminal 6x- Histidine-tag using the vector pET-28 a(+) vector. **(B) Cloning of *L.***
1193 ***donovani* SphK1 in pET28a(+) vector.** PCR amplification of DNA fragment from genomic
1194 DNA of *L. donovani* using *Ld*Sphk1_BamHI and *Ld*Sphk1_XhoI with Phusion™ High-
1195 Fidelity DNA Polymerase. Purification of the amplified DNA fragment was done using
1196 QIAquick Gel Extraction Kit followed by digestion of purified *Ld*Sphk1 insert and the
1197 expression vector pET-28 a(+) with BamHI/XhoI restriction enzymes. The positive clones
1198 were screened by colony PCR followed by confirmation of the cloned plasmid with
1199 BamHI/XhoI restriction digestion. **(C) *rLd*Sphk1 recombinant protein purification**.
1200 Transformation of positive clone in Rossetta *E. coli* expression strain for *Ld*Sphk1 recombinant
1201 protein expression. For recombinant protein induction, the cells were induced with 1mM IPTG
1202 for 4 hours at 37°C in Terrific broth. Purification of recombinant protein was achieved
1203 by affinity chromatography. The *rLd*SphK1 protein was eluted after addition of 150mM
1204 imidazole solution. The eluted fractions were analysed by running on 12% SDS PAGE.
1205
1206 **Fig S2. (A) The Human SphK1 amino acid sequence for the protein. (B) Purification of**
1207 **the recombinant *Human*SphK1 (*rHuman*SphK1) protein.** Overexpression of 6×His-SphK-
1208 1 (*rhSphK-1*) was induced with 1mM IPTG at an optical density (OD600) of 0.6, for 4 h at
1209 37°C. The protein was purified using Ni-NTA agarose resin. The *rhSphK1* protein was eluted
1210 with a continuous imidazole gradient of 50mM, 100mM, 250mM, and 500mM. The protein
1211 purification was validated by 12% SDS-PAGE, followed by immunoblotting with anti-His tag
1212 antibody. A single band corresponding to ~50 kDa was observed on SDS PAGE corresponding
1213 to Human specific SphK1.
1214

1215 **Fig S3. (A,B) Effect of SphK1 inhibitors; SKI-5C and DMS in *Leishmania promastigotes*.**
1216 To evaluate the IC_{50} for SKI-5C and DMS, approximately 5×10^4 *Ld* Bob cells were seeded in
1217 each well of 96-well flat bottom plates and supplemented with M199 media containing SKI-
1218 5C and DMS (200µl/well) respectively. The cells were further incubated for 2 days at 37°C
1219 and 5% CO_2. The IC_{50} were found to be 100µM for SKI-5C and 500µM for DMS respectively
1220 in *Leishmania donovani* promastigotes. Each experiment was done in triplicates and repeated
1221 thrice. **(C) Effect of SphK1 inhibitor; ABC294640 in *Leishmania spp* and host**
1222 **macrophages.** To evaluate the IC_{50} for ABC294640, approximately 6×10^3 THP-1 and 5×10^4
1223 *Ld* Bob cells were seeded in each well of 96-well flat bottom plates and supplemented with
1224 RPMI and M199 media containing ABC294640 (200µl/well) respectively. For intracellular
1225 amastigotes, 1×10^6 THP-1 cells, treated with 50 ng/ml of phorbol 12-myristate 13-acetate
1226 (PMA) were seeded on glass coverslip in a 6-well plate for 48h. They were infected with late
1227 log-phase *L. donovani* promastigotes and simultaneously treated with ABC294640. The cells
1228 were further incubated for 2 days at 37°C and 5% CO_2. To determine, the intracellular parasite
1229 burdens (mean number of amastigotes per macrophage) were microscopically assessed using
1230 Giemsa staining. For axenic amastigotes, the axenically cultured forms grew optimally at a
1231 temperature of 32-33°C in a growth media with pH of 5.4. The IC_{50} were found to be 60µM
1232 for THP-1 macrophages and 69.7µM for intracellular amastigotes respectively. Each
1233 experiment was done in triplicates and repeated thrice.
1234
1235 **Fig S4. (A) Amino acid sequence alignment of LD_SphK1 and Human_SphK1 utilizing**
1236 **MEGAX program (version 10.2.2).** The results demonstrated considerable alignment with
1237 similar and a limited number of identical amino acids. **(B) 3D structural alignment of**
1238 **LD_SphK1 and Human_SphK1 protein structures with Pymol software.** Substantial
1239 alignment between the two proteins, with an RMSD of 0.585 was observed. Furthermore, the

1240 alpha helix and beta sheets of the Human DAGKc domain (Blue) accurately aligned with the
1241 LD_DAGKc domain (Yellow). **(C) Construction of phylogenetic tree utilizing SphK1 gene**
1242 **sequences from various species of *Leishmania,* humans, rats, and mice.** The phylogenetic
1243 tree was constructed using neighbor-joining technique with MEGAX software. Bootstrap
1244 analyses with 1000 replicates were conducted to evaluate the robustness of the constructed
1245 phylogenetic tree.

1246 **Fig S5. (A) Effect of Ceramide analogs; DL-threo-PPMP and DL-erythro-PPMP in THP-**
1247 **1 macrophages.** To evaluate the IC_{50} for DL-threo-PPMP and DL-erythro-PPMP,
1248 approximately 6×10^3 THP-1 cells were seeded in each well of 96-well flat bottom plates and
1249 supplemented with RPMI media containing DL-threo-PPMP and DL-erythro-PPMP
1250 (200µl/well) respectively. The cells were further incubated for 2 days at 37°C and 5% CO_2.
1251 The IC_{50} were found to be 19.53µM and 116µM for DL-threo-PPMP and DL-erythro-PPMP
1252 respectively in THP-1 macrophages. Each experiment was done in triplicates and repeated
1253 thrice.

1254 **Table S1. Primer sequences of target genes mentioned along with their annealing**
1255 **temperatures**